KfK 4590
Februar 1991

The Hybrid K - Edge / K - XRF Densitometer: Principles - Design - Performance

H. Ottmar, H. Eberle
Institut für Kernphysik
Projekt Wiederaufarbeitung und Abfallbehandlung

Kernforschungszentrum Karlsruhe

Kernforschungszentrum Karlsruhe

Institut für Kernphysik

Projekt Wiederaufarbeitung und Abfallbehandlung

KfK 4590
PWA 01/91

The Hybrid K - Edge / K - XRF Densitometer : Principles - Design - Performance

H. Ottmar, H. Eberle

Kernforschungszentrum Karlsruhe GmbH, Karlsruhe

Als Manuskript gedruckt

Kernforschungszentrum Karlsruhe GmbH
Postfach 3640, 7500 Karlsruhe 1

ISSN 0303-4003

Abstract

The Euratom Safeguards Directorate (ESD) has recently installed a hybrid K-edge/K-XRF densitometer in a commercial reprocessing plant for the safeguarding of nuclear materials. This instrument, developed at KfK Karlsruhe, offers for the first time analytical measurement capabilities for timely on-site input accountancy verification. Lectures providing informations on measurement principles, instrument design features and performance data have been given to inspectors of ESD to make them familiar with the new instrument. This report summarizes the essential materials presented during these courses.

Das kombinierte K-Absorptiometrie/K-Röntgenfluoreszenz-Spektrometer : Meßprinzip - Auslegung - Leistungsdaten.

Zusammenfassung

Die Direktion Sicherheitsüberwachung von Euratom hat für ihre Verifikationsmessungen zur Kernmaterialüberwachung ein Hybrid-Röntgenspektrometer in einer kommerziellen Wiederaufarbeitungsanlage installiert. Das im Kernforschungszentrum Karlsruhe entwickelte Gerät bietet erstmals die Möglichkeit, analytische Messungen an den hochradioaktiven Eingangslösungen vor Ort durchzuführen. In Trainingskursen wurden Inspektoren von Euratom mit den methodischen und instrumentellen Merkmalen des Spektrometers vertraut gemacht. Die wesentlichsten Inhalte der in diesen Kursen vermittelten Informationen sind in diesem Bericht zusammengefaßt.

Contents

1. Introduction

In November 1989 the Euratom Safeguards Directorate (ESD) has installed a Hybrid K-Edge / K-XRF Densitometer at the reprocessing plant of La Hague, France. The instrument, developed at KfK Karlsruhe /1,2,3/ and delivered under a licence agreement by Canberra-Packard GmbH, Frankfurt, is designated for the independent verification of the uranium and plutonium element concentration in dissolver solutions from the new plant UP3. The respective verification measurements are now being carried out routinely by inspectors of ESD. With the installation and operation of this densitometer there exist now, for the first time, analytical measurement capabilities for timely *on-site* input accountancy verification in a reprocessing plant.

With the existing instrument we come fairly close to a situation for the analytical input accountability measurements as envisaged at the beginning of its development (Fig. 1). In fact, the installed densitometer offers significant improvements both in terms of operational simplicity and speed of analysis compared to the analytical practice encountered in the traditional approach using Isotope Dilution Mass Spectrometry (IDMS). With the Hybrid Instrument the input measurements are carried out in a fairly simple and straightforward manner, requiring only a few user interactions. These are specified in a concise operations guide provided with the instrument. When following the given instructions, also non-specialists will be able to run a measurement.

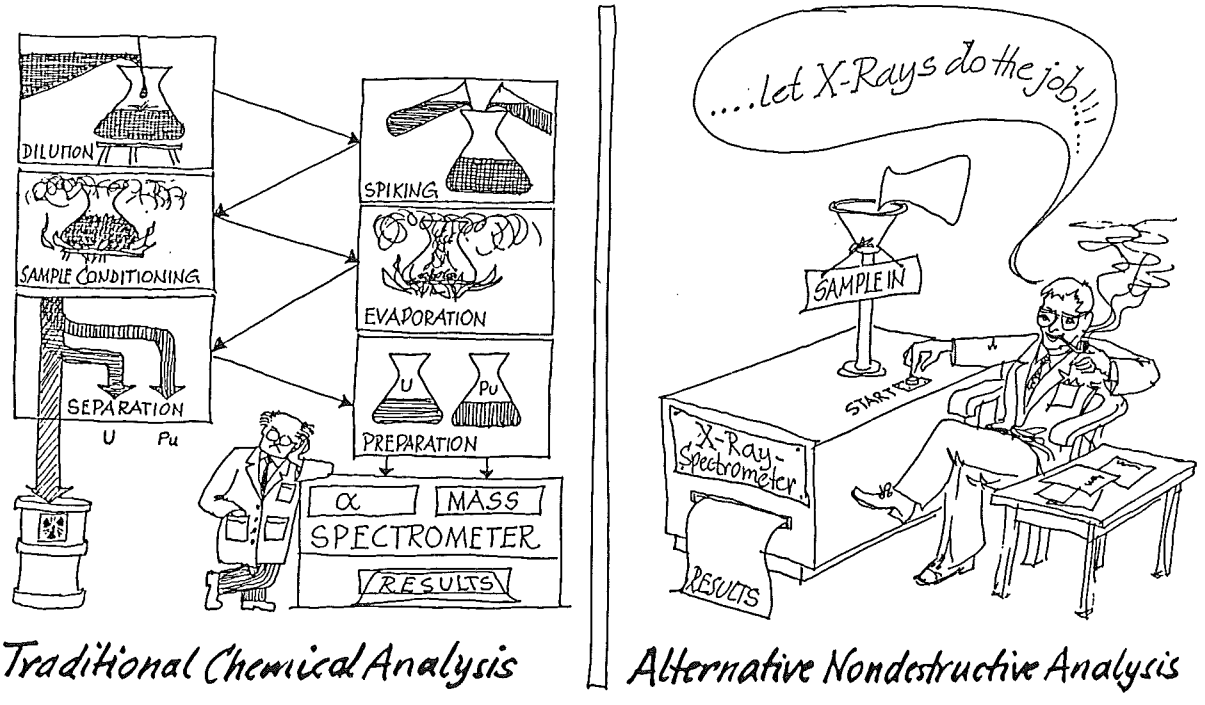

Fig. 1 : Approaches to reprocessing input measurements.

In this way the analytical input measurements have become a relatively easy task. Nevertheless, it appeared desirable that the safeguards inspectors operating the instrument should have some basic knowledge about the underlying measurement process in order to be able to better assess the various instrument responses and to gain increased assurance and confidence of their measurements.

To this end lectures have been presented to inspectors of ESD which outlined the basic physical principles of the incorporated measurement techniques, the major design features of the instrument's hardware and software, and the crucial measurement items that ultimately determine the overall uncertainty and reliability of the uranium and plutonium assay in the dissolver solutions. This report summarizes the essential materials presented during these courses. Those informations concerning some basic physical facts and data, which can be found, of course, also in textbooks, are added for the sake of completeness in the Appendices. The latter also contain some typical data on dissolver solutions (Appendix G) as well as results from a preliminary instrument calibration (Appendix H).

2. The Instrument

2.1 Measurement Techniques

To determine the uranium and plutonium concentration in input solutions, two separate sample vials - each containing about 1 mℓ of the solution to be analyzed - are irradiated with high-intensity X-ray beams from an X-ray tube as shown in Fig. 2. The interrogating X-ray beams are utilized in two different manners:

- First, the transmission of a highly collimated X-ray beam passing through a solution sample of well-defined path length (glass cuvette) is measured as a function of energy in critical energy regions. The underlying measurement technique is K-absorption edge spectrometry, colloquially called K-edge densitometry (KED). This technique is used to determine the uranium concentration.
- Second, another X-ray beam of larger divergence irradiating a second sample vial (PE vial) stimulates the emission of characteristic X-rays from uranium and plutonium in the input solution. The intensities of these induced X-rays are measured and used to determine the U/Pu ratio. The underlying measurement technique is the well-known technique of X-ray fluorescence (XRF) analysis.

Both the KED and XRF measurements are carried out simultaneously. The required instrumentation is - except for the X-ray generator - identical to that typically used in gamma-ray spectrometry.

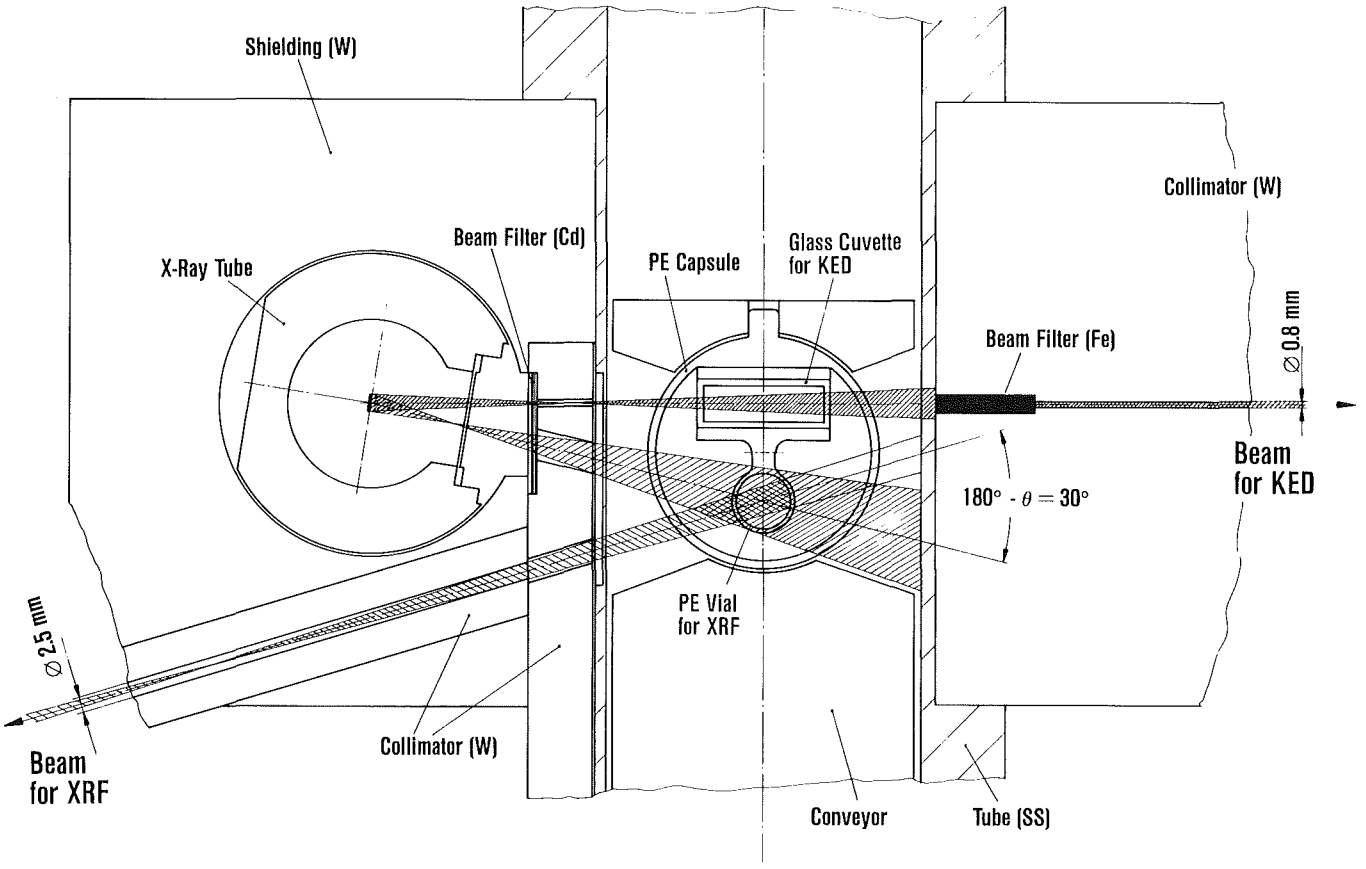

Fig. 2 : Plan of the X-ray beam geometry for KED and XRF in the Hybrid Instrument (Scale 1 : 1.25).

2.2 Instrument Configuration

2.2.1 Mechanical Set-up

The instrument is installed at a shielded cell, in which the input solutions are received by means of a pneumatic posting system. At the backside of the shielded cell an entrance port to the cell was available, where the instrument could be adapted.

The drawing in Fig. 3 represents a horizontal cross-sectional view of the mechanical set-up. The actual mechanical assembly is shown on the photograph in Fig. 4, which was taken prior to the instrument installation. The stainless steel tube with an outer diameter of 8 cm is penetrating the box shielding and fits into an existing flange of the box as indicated in Fig. 3. The inside of the

tube has a rectangular profile to accommodate a sledge used as sample conveyor. The photograph in Fig. 5 shows the end section of the tube extending into the box, with the sledge at the sample loading position.

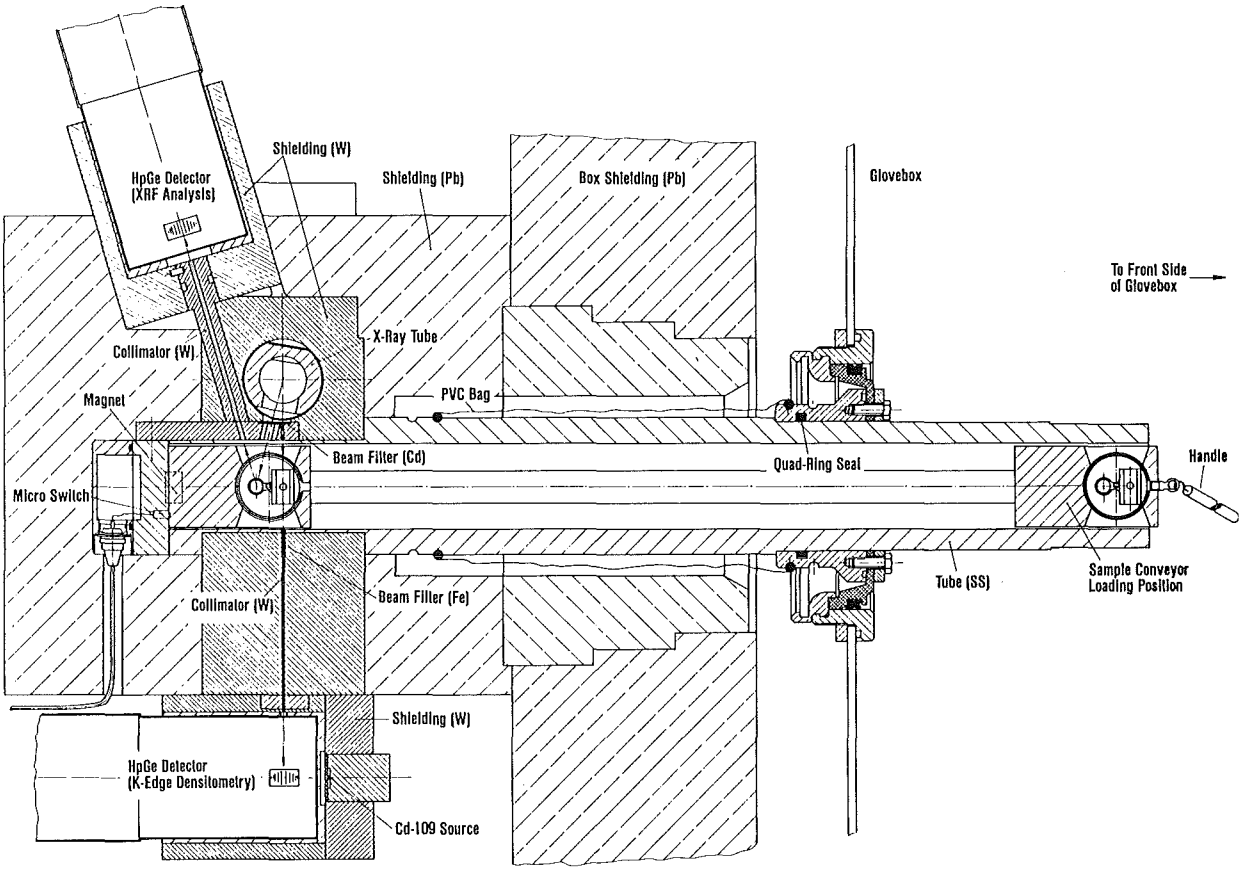

Fig. 3 : Plan of the Hybrid Instrument installation at the reprocessing plant of La Hague (Scale 1 : 4.5).

The sledge, which is easily gliding inside the tube, is pushed manually over the relatively short distance of about 50 cm from the sample loading position to the measurement position in the instrument. In the latter position it is held by means of a small magnet. A microswitch is actuated when the sample conveyor has reached its correct position for a measurement.

The primary shieldings for the X-ray tube and the detectors, and the beam collimators are fabricated from a tungsten alloy. For the measurement of the highly radioactive dissolver solutions it is important to keep the distance between the X-ray tube and the samples as short as possible. Therefore the configuration has been designed as compact as possible, achieving a distance of

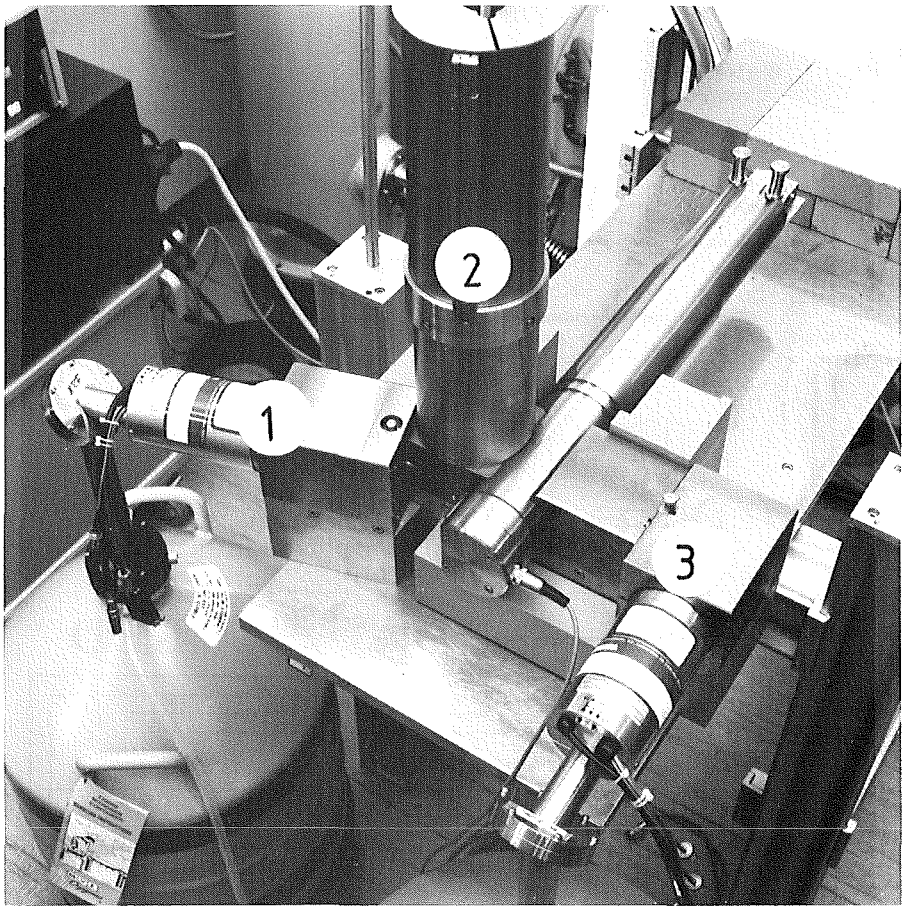

Fig. 4 : *Mechanical set-up of the Hybrid Instrument prior to installation. (1) XRF detector, (2) X-ray tube, (3) KED detector.*

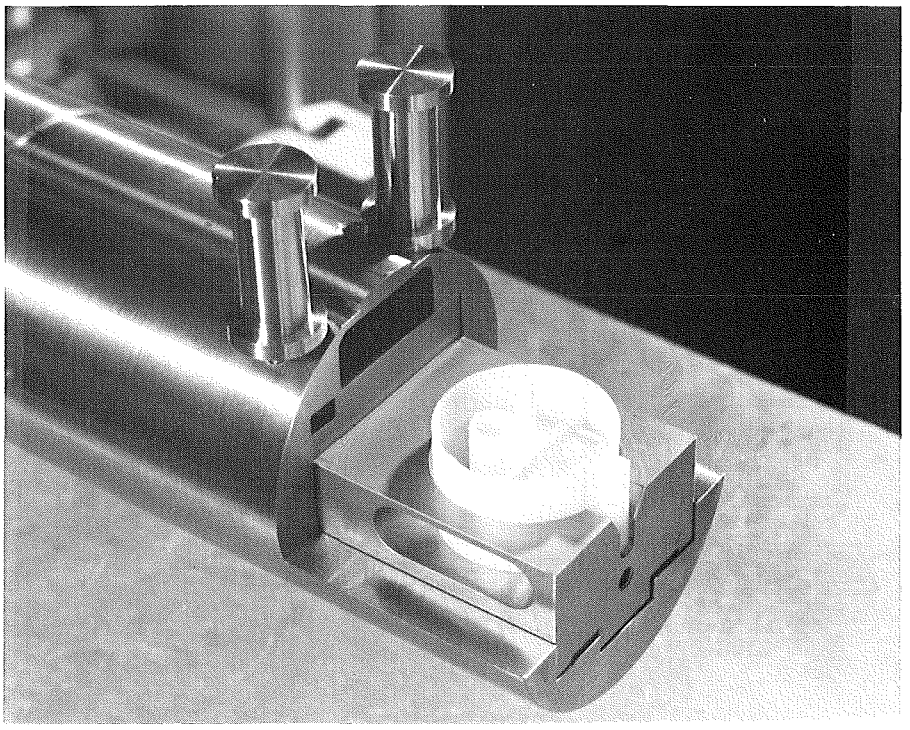

Fig. 5 : *Tube section extending into the shielded cell. Sample conveyor with PE capsule (cover removed) at the loading position.*

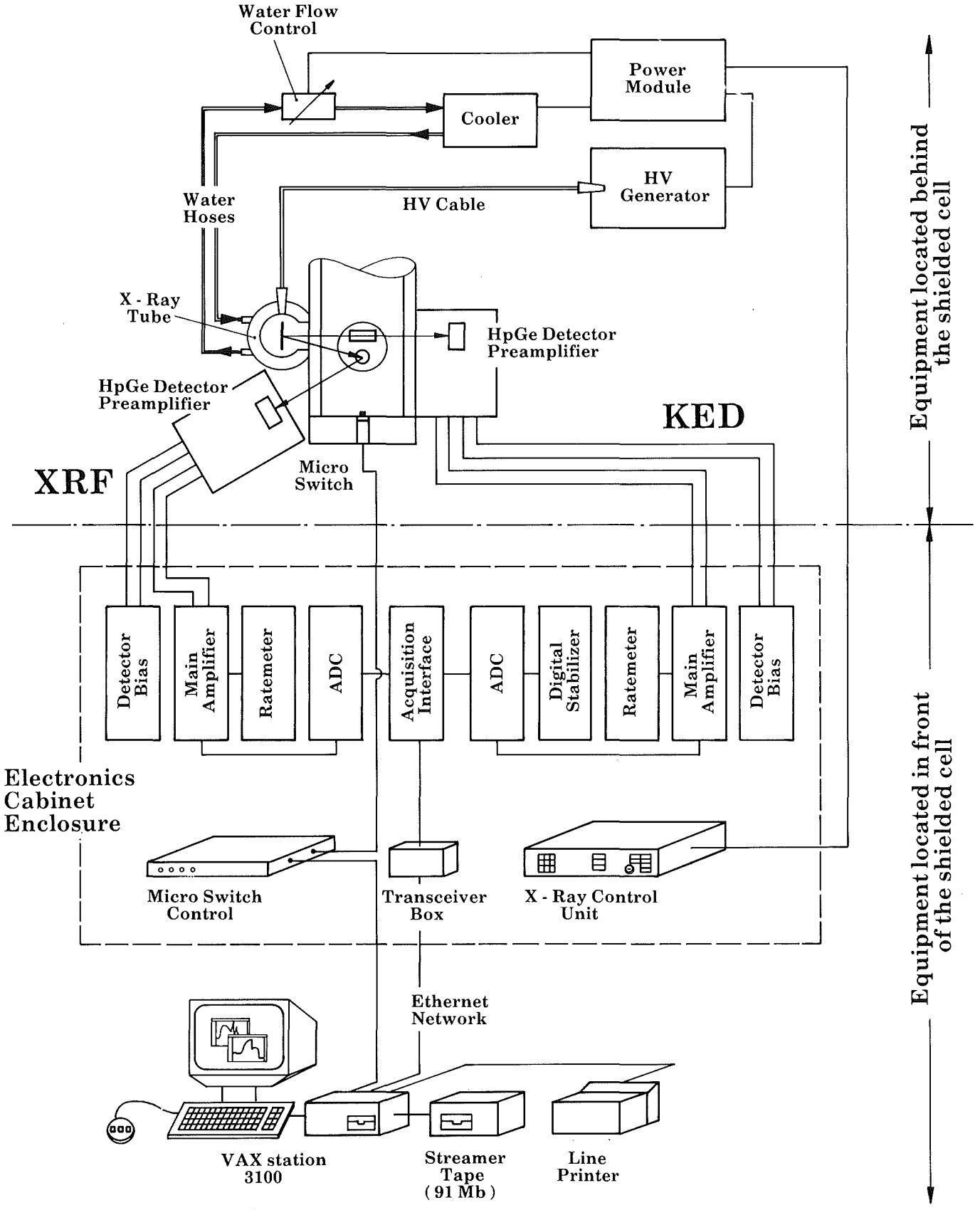

Fig. 6 : Block diagram of the instrument components.

6.5 cm between the focal spot of the X-ray tube and the center axis of the stainless steel tube.

The straight-through beam for KED passes a total thickness of 20 mm of Fe. There is an additional filter of 1 mm of Cd placed next to the X-ray tube (see Fig. 2), which filters both beams used for KED and XRF. The tungsten shielding block between sample and KED detector has a 10 cm long collimator hole with a diameter of 0.8 mm. Because of space limitations at the site of installation, the axis of the cryostate for the KED detector had to be orientated perpendicular to the incoming X-ray beam as shown in Fig. 3. This special geometry also necessitated to turn the Ge crystal inside the cryostate by 90° against its standard mounting position to allow irradiation through the side of the detector cap. The ^{109}Cd-source located close to this detector serves as reference source for digital stabilization of the analogue electronics.

The XRF detector is orientated at a backward angle of 150° relative to the direction of the respective primary X-ray beam. The tungsten collimator in front of the XRF detector has a diameter of 2.5 mm and a length of 10 cm.

The mechanical assembly is mounted on a small table right at the periphery of the box shielding. It is surrounded by a layer of 10 cm of lead, which provides sufficient shielding against the high-energy gamma radiation from the dissolver solution sample when it is at the position for measurement outside of the shielded glovebox.

2.2.2 Instrument Components

The block diagram of the complete set-up (Fig. 6) shows the different components of the instrument, how they are interconnected, and where they are located. All items are commercially available components.

The equipment located behind the shielded cell comprises the mechanical set-up, two planar HpGe-detectors (200mm^2 x 10 mm) for XRF and KED, and the X-ray tube with associated power modules. The X-ray tube - a metal-ceramic tube with tungsten target - is operated at 150 kV/15 mA, which corresponds to about 75% of its maximum power rating of 3 kW. An air-cooled water circulator provides the required cooling for the X-ray tube.

The equipment located in the working area in front of the shielded box comprises an electronics cabinet containing the NIM modules for the detectors, the X-ray control unit and the microswitch control unit. The NIM modules for the two detector systems are contained in a single NIM bin. The respective modules

are identical for both detectors, except that the branch for the KED detector also includes a digital stabilizer.

An Ethernet-based spectroscopy workstation with associated periphery is used for data acquisition and analysis. It includes an Acquisition Interface Module (AIM) with built-in IEEE 802.3/802.2 conforming Ethernet (LAN) Interface connected to a Digital VAX station 3100. The latter runs under Digital Micro VMS Operating System and includes Micro VMS workstation software providing multi-windowing capabilities. The dedicated software packages for spectrum analysis and data evaluation are written in FORTRAN.

2.2.3 Sample Vials

In order to optimize both the KED and the the XRF measurement, separate sample vials are used for the two methods. The X-ray beam for KED passes through a rectangular-shaped glass cuvette with accurately known path length ($d = 20 \pm 0.002$ mm). For XRF a thin-walled cylindrical PE vial with an inner diameter of 9 mm is used. Both vials are mounted on a sample holder (PE), which in turn is placed into a PE capsule for the measurement. The photograph in Fig. 7 shows the vial holder and the PE capsule loaded into the sample conveyor.

The drawing given before in Fig. 2 detailed the X-ray beam geometry for the two measurements. The collimators in front of the K-edge ($\varnothing = 0.8$ mm) and XRF detector ($\varnothing = 2.5$ mm) are much narrower than the cross-sections of the primary beams impinging on the two vials. The actual portions of solution seen by the detectors are indicated in Fig. 8 as black areas. The beam axis for K-edge densitometry is located 3 mm above the bottom of the glass cell, whereas the beam axis for XRF intercepts the PE vial 7 mm above its bottom.

For KED it is mandatory that the full beam diameter seen by the detector has crossed the solution. If this requirement is not fulfilled, the measurement becomes invalidated, yielding too low concentrations. Consequently, the glass cuvette must be filled to a level where the meniscus of the solution surface at its minimum is at least 5 mm above the bottom of the cuvette. It is recommended to fill the glass cuvette , which has an internal width and height of 6 mm and 10 mm, respectively, with about 1 mℓ of input solution. The same quantity of solution should also be filled into the PE vial for the XRF measurement.

The vials are not tightly closed when put into the PE capsule. Consequently, evaporation of the solution may occur, causing an increase of the

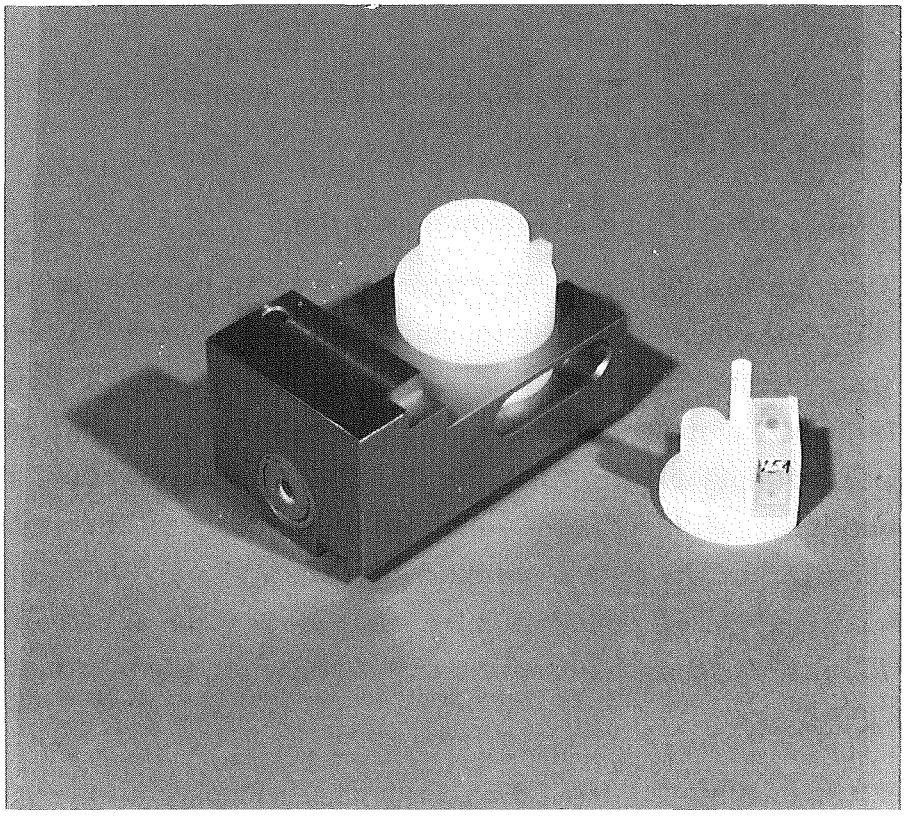

Fig. 7 : *Photograph of sample vials (right) and PE capsule loaded into the sample conveyor.*

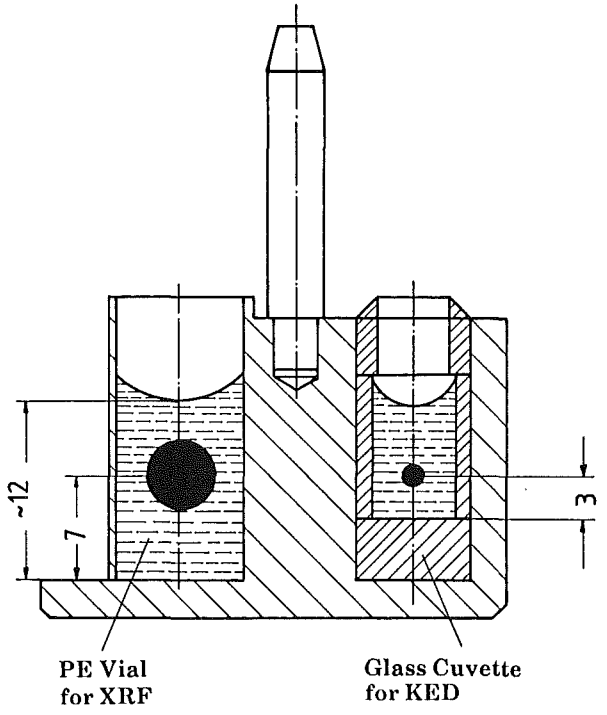

Fig. 8 : *Sample holder with PE vial for XRF and glass cuvette for KED. The black dots indicate the portion of solution seen by the respective detector.*

concentration. Therefore the input solution should be measured immediately after it has been transferred into the vials.

2.2.4 Test Samples for Measurement Control

Two test samples - a sealed glass cuvette containing a uranium solution and a (U, Pu) MOX-pellet welded in stainless steel - were prepared by the European Institute for Transuranium Elements, Karlsruhe /4/. Both samples serve for the purpose of measurement control to check the instrument stability for KED and XRF, but not for calibration. The MOX pellet contains about 5% Pu with a ^{239}Pu abundance of 98.3%. The very low abundance of the isotope ^{241}Pu (0.097 %) ensures that the plutonium mass decreases by only 0.0046 % per year due to the natural decay. Consequently, the U/Pu ratio effectively remains constant for longer periods. The uranium concentration in the solution sample for KED is 218 gU/ℓ.

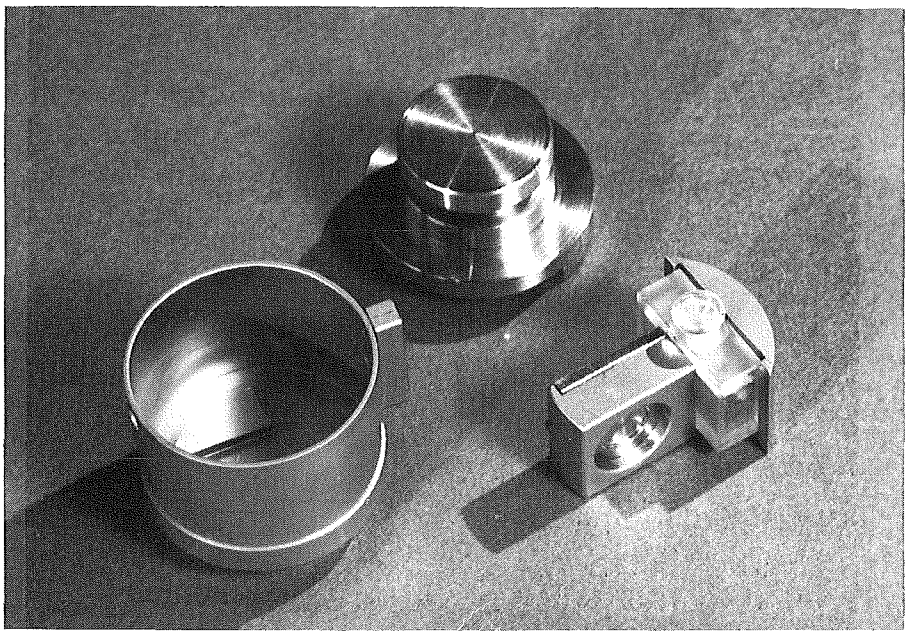

Fig. 9 : Stainless steel capsule with reference samples for measurement control.

The two test samples are mounted into a frame and located in a stainless steel capsule as shown in Fig. 9. The stainless steel capsule is loaded into the sample conveyor in the same manner as the PE capsule containing the input solution. For a counting time of 1000 s the measurement precision obtained for the

uranium concentration from KED is 0.22%. A similar precision (0.24%) is also obtained for the U/Pu ratio measurement on the MOX pellet from XRF.

2.3 Measurement Procedure

Only a few user actions are necessary for the execution of a measurement. The user has

- to transfer approximate aliquots of about 1 mℓ into the vials for XRF and KED, to load the samples into the conveyor, and to push the conveyor into the measurement position. The accumulation of spectral data can only be started when the microswitch controlling the conveyor position has been actuated. The operations inside the shielded cell are carried out by staff members of the plant operator and observed by inspectors ;
- to switch on the X-ray unit. A programmed warm-up mode for tube conditioning (about 5-20 minutes, depending on the period elapsed since the last operation), is recommended before the unit is set into the normal operating mode at preset operating values (150 kV, 15 mA) by pressing a single push-button ;
- to log in at the workstation and to step through the outlined procedure. The menu presented offers the option for a measurement (KED, XRF or both) or for a post evaluation of previously accumulated spectra. When requesting a measurement, the type of the sample - test samples or input solution - has to be specified. For a control measurement on the test samples no further inputs are required. For a measurement on an input solution the user is prompted for the following inputs :
  - Sample identification ;
  - ^{235}U enrichment, if known ;
  - Density of the solution, if known ;
  - Temperature inside the shielded cell ;
  - Number of desired repeat runs;
  - Counting time.

The sequence of actions, and the critical items and instrument responses to be observed, are listed in the operations guide. The data acquisition, once initiated, and the subsequent data evaluation run under automated procedures. Details of the measurements will be discussed in the chapters below.

Upon the completion of a measurement, the operator pulls the sample conveyor back into the shielded cell and unloads the samples. The sample vials are emptied and disposed, whereas the PE container is re-used for some time.

3. K-Edge Densitometry Measurement

3.1 Features of the K-Edge Spectrum

The X-ray continuum passing through the glass cuvette for KED is suitably tailored by means of beam filters (1 mm Cd, 20 mm Fe). The top curve in Fig. 10 shows the original X-ray continuum emitted by the tube, which is operated at 150 kV/15 mA. The bottom curve in the figure represents the tailored beam reaching the detector if there is no solution sample in the beam path. The photon distributions shown in the figure were calculated using an analytical expression for photon spectra from X-ray tubes given in Ref. 5 (see Appendix E), and mass attenuation coefficients tabulated in Ref. 6.

Examples of actual spectra recorded by the K-edge detector are shown in Fig. 11. The spectra are accumulated into 2 K channels and cover the energy range from 0 to 185 keV. The figure displays in a logarithmic vertical scale the spectral distribution for a blank (3 N HNO_3) solution and for a typical input solution. In both cases the cell length was 2 cm. Note in the spectrum from the input solution the characteristic jump of the photon transmission at the K-absorption edge energy of uranium (115.6 keV). The height of the jump is a measure for the uranium concentration in the solution. Fig. 12 shows the typical jump for 4 different concentrations (note the logarithmic scale). The spectra in this figure may guide the user to obtain just from a simple visual inspection of the K-edge spectrum an indication of the approximate magnitude of the uranium concentration in the sample.

There appear a few gamma and X-ray peaks in the spectra of Fig. 11. The peaks at 22.10, 25.00 and 88.04 keV originate from the ^{109}Cd-source located close to the detector (see Fig. 3). The first and the latter peak are used as reference peaks for the digital stabilization of the electronics. The tungsten X-rays originate both from the X-ray tube and from the tungsten material used for collimation and shielding. The lead X-rays observed in the spectra arise from lead impurities in the aluminium detector cap.

Further we note from Fig. 11 that the spectra do not fall off towards zero intensity on the low-energy side of the X-ray continuum as expected from the photon distribution shown in Fig. 10. This is because a significant fraction of X-

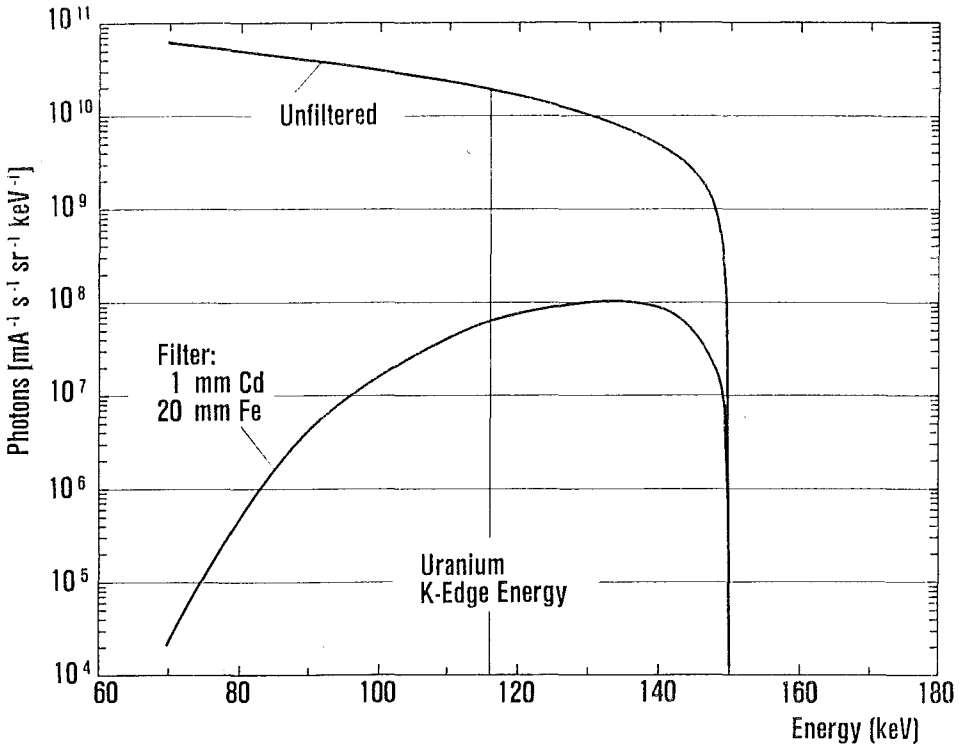

Fig. 10 : X-ray continuum emitted by the X-ray tube (top) and tailored spectrum for KED (bottom).

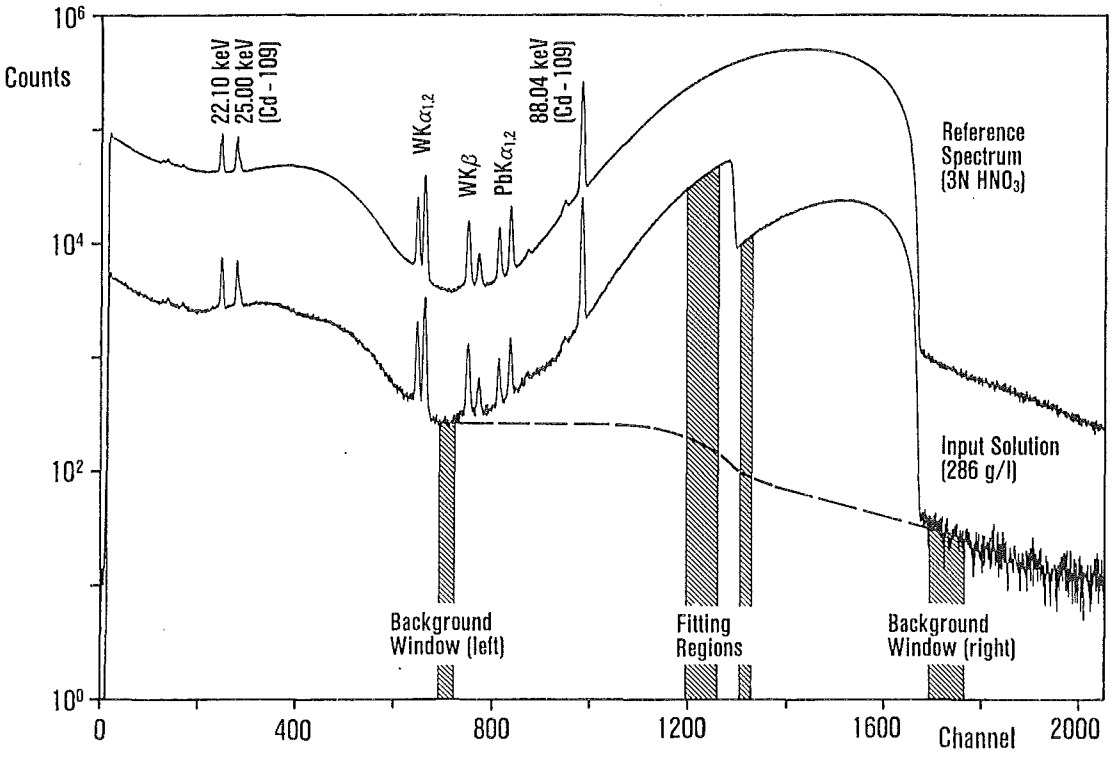

Fig. 11 : Characteristic spectra recorded by the K-edge detector from a blank solution (top) and from an input solution (bottom).

ray photons reaching the detector become inelastically scattered, leaving part of their incident energy in the detector. The counts recorded in the first 600 to 800 channels of the spectrum are due to such inelastic scattering events in the Ge detector.

Similarly, the X-ray continuum also does not drop to zero at its high-energy side. The counts observed above the cut-off energy of the X-ray continuum represent events due to pulse pileup in the pulse processing electronics. The cut-off energy of the X-ray continuum (150 keV) is equivalent to the potential applied to the X-ray tube (150 kV). Note that the K-edge spectrum offers the possibility to measure and to control the actual tube voltage very accurately (to about 0.1%) from the cut-off energy of the X-ray continuum.

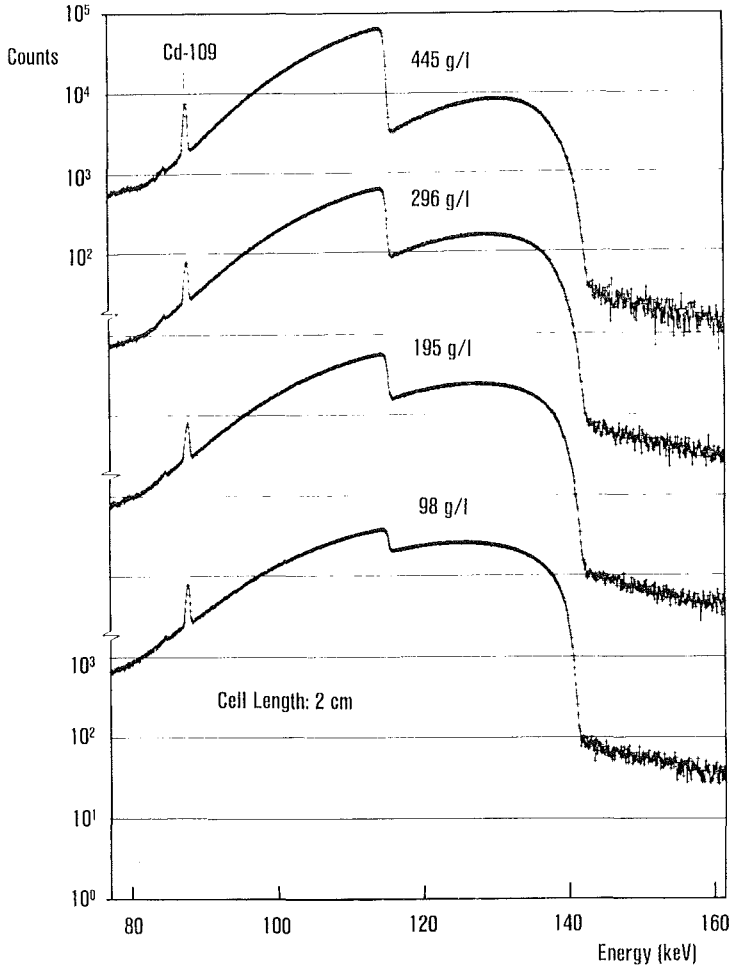

Fig. 12 : K-edge jump for different uranium concentrations.

3.2 Counting Rate

With increasing uranium concentration the transmitted X-ray beam becomes increasingly attenuated. Hence, the counting rate of the K-edge detector will decrease with increasing uranium concentration for a fixed tube current. This is shown in Fig. 13 (note the different behaviour of the counting rate in the XRF detector also shown in the figure, which slightly increases with increasing uranium concentration). For a given uranium concentration, and for the adopted settings of the X-ray tube (150 kV/15mA), the counting rates observed in both detectors should be in accordance with the values read from Figure 13.

With a blank nitric acid solution the counting rate in the K-edge detector will increase to about 75 kcps, if the tube current is kept constant at 15 mA. To reduce this rate, the reference spectrum shown in Fig. 11 was accumulated with a tube current of 5 mA.

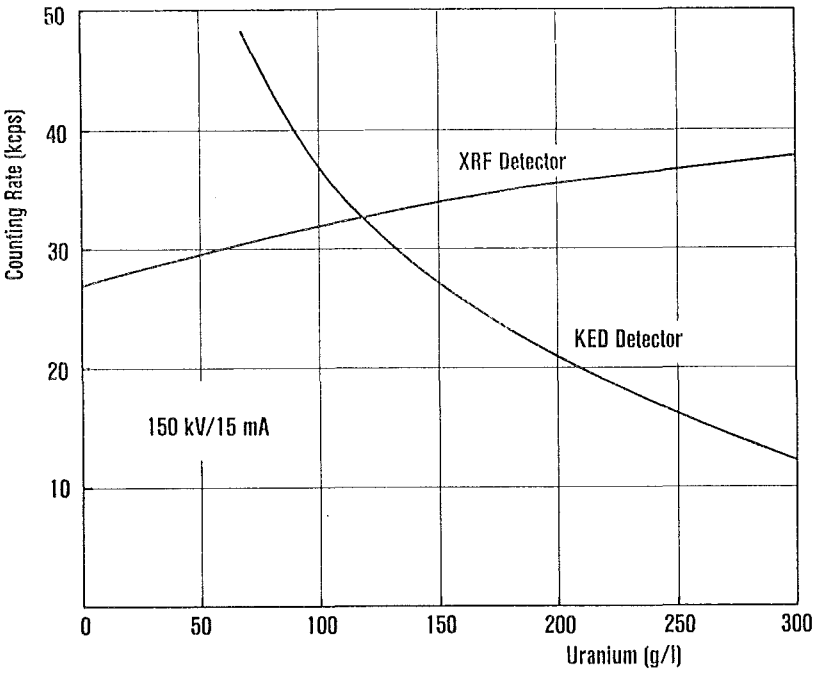

Fig. 13 : Counting rates for the KED and XRF detector as a function of the uranium concentration.

3.3 Spectrum Analysis

3.3.1 Check of Spectral Parameters

After the acquisition of a K-edge spectrum the software for spectrum analysis checks the following items:

Position of Reference Peaks. The channel positions of the two reference peaks for digital stabilization (22.10 and 88.04 keV lines from ^{109}Cd) are determined using a routine for peak fitting. The routine computes a least-squares fit with a parabolic function to the logarithmic counts of the 5 top peak channels. A new energy calibration is made for each spectrum from the actual peak position of the reference peaks. Since the electronics for KED is digitally stabilized, the channel positions of the two reference peaks (246 and 982, respectively) should remain constant within ± 0.1 channels.

Detector Resolution. The detector resolution is monitored from the FWHM of the 88.04 keV line. The FWHM-value is obtained from the previous peak fitting routine. The nominal FWHM-value is 520 ± 10 eV.

Control of High Voltage for X-Ray Tube. The high voltage is monitored from the cut-off energy of the X-ray continuum. The onset of the continuum is determined from the spectral counts in the energy region around 150 keV. The value reported in the protocol under the item ' HV control ' is determined from the energy of the channel where the counts exceed 10 times the standard deviation of the average pileup background in the energy bin 150.6 - 151.4 keV. The nominal HV-control value is 149.6 ± 0.1 kV.

3.3.2 Background Subtraction

For a correct determination of the photon transmission the background underneath the X-ray continuum must be removed in the energy region of interest. The background arises - as mentioned in Sect. 3.1 - from pulse pileup and inelastic scattering. The background is approximated by a smooth transition between the background levels on both sides of the X-ray bump as indicated in Fig. 11. The calculated background has the following form /7/ :

$$BG(I) = B_L + (B_R - B_L) \cdot \sum_{j=L}^{j=R} Y(j) \; / \; \sum_{K=L}^{K=R} Y(K) \qquad (1)$$

where

BG(I) = computed background at channel I

Y (I) = spectra counts of channel I

B_L = average counts in left background window (61.8 - 64.8 keV)

B_R = average counts in right background window (151.9 - 158.4 keV).

3.3.3 Normalization to Reference Spectrum

The photon transmission of a sample is measured relative to the photon distribution in a reference spectrum obtained from a blank sample

(3N HNO_3). This spectrum - once measured after the instrument installation - is permanently stored in the system and called for the evaluation of each KED measurement.

The adopted procedure for the evaluation of the K-edge jump (see Sect. 3.3.4) requires that the transmission spectra for the input sample (S) and for the blank reference sample (R) are normalized to each other for equal numbers of incident photons. The normalization has to account for the different counting times t_S, t_R and tube current settings I_S, I_R, and for the effective X-ray production rates P_S, P_R of the X-ray tube during the measurement of the reference and the sample. The normalized ratio of counts

$$\left(\frac{N_R}{N_S}\right)_{norm} = \left(\frac{N_R}{N_S}\right)_{meas} \cdot \frac{ts}{t_R} \cdot \frac{Is}{I_R} \cdot \frac{Ps}{P_R} \qquad (2)$$

is determined from the ratio of spectral counts at a given energy E. Using the counting times t_S, t_R, which are known as input parameter, the routine for normalization calculates the remaining factor $(I_S \cdot P_S)/(I_R \cdot P_R)$ from the accumulated counts N_R, N_S at energy E = 118.7 keV, taking into account the additional photon attenuation in the input sample. At the normalization energy, purposely chosen just above the K-absorption edge of uranium (E_K = 115.6 keV), the additional photon attenuation in the input sample is almost exclusively determined by the uranium concentration. Hence, it is calculated to $\exp - [\mu_u \cdot \rho_u \cdot d]$, with μ_u = mass attenuation coefficient for uranium at 118.7 keV, ρ_u = uranium concentration, and d = cell length. The value for μ_u (4.7 $cm^2 g^{-1}$) is included into the parameter file for KED.

The normalization factor appearing in the protocol corresponds to the value of

$$\alpha = \ell n \frac{I_S \cdot P_S}{I_R \cdot P_R} \qquad (3)$$

The specific X-ray production rates P_S, P_R may differ by a few percent at maximum. Hence, α approximately equals to the logarithmic ratio of the tube current settings I_S and I_R. With the present settings I_S = 15 mA, I_R = 5 mA, we expect a value of $\alpha \approx 1.10$.

3.3.4 K-Edge Jump of the Photon Transmission

The K-edge jump of the photon transmission is determined from spectral data in two energy windows below and above the absorption edge. The two windows indicated in Fig. 11 cover the energy regions 107.2 - 113.2 keV and

117.2 - 119.5 keV, respectively. The smaller window width above the absorption edge was chosen to exclude the nearby absorption edge of plutonium at 121.8 keV as illustrated in Fig. 14 for a solution with a U/Pu ratio of ~ 3. In the transmission spectrum from an input solution, however, the plutonium edge is practically not visible (see Fig. 11) because of the much lower concentration of plutonium.

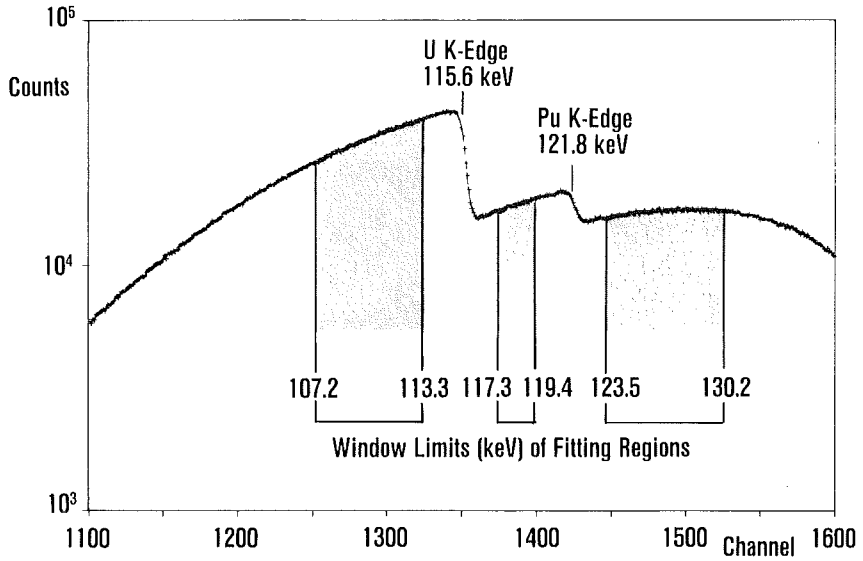

Fig. 14 : Transmission spectrum for a solution with a U/Pu ratio of about 3 (156 gU/ℓ, 51 g Pu/ℓ).

The evaluation of the K-edge jump of the photon transmission includes the following steps:

1. Subtraction of the background in the reference spectrum and in the spectrum from the measured sample as described in Sect. 3.3.2.

2. Normalization of the background corrected counts as described in Sect. 3.3.3.

3. Calculation of the inverse transmission values channel by channel within the windows below and above the absorption edge E_K :

$$1/T = YNET_R / YNET_S \quad , \tag{4}$$

where the subscripts R and S refer to the counts in the reference spectrum (R) and in the spectrum from the sample (S).

4. Linearization of the experimental data. In Appendix B, Eq. B 8 it was shown that the relation

$$\ell n\, \ell n\, 1/T = a - b\, \ell n E \tag{5}$$

holds. Defining

$$Y(i) = : \ell n\, \ell n\, 1 / T(i) \tag{6}$$

$$X(i) = : \ell n E(i) - \ell n E_{\ell} \tag{7}$$

where E(i) denotes the energy of channel number i and $E\ell$ the energy of the window limit next to the edge, we obtain the linear relation

$$Y(i) = A_0 - A_1 X(i) \quad . \tag{8}$$

An example of the linearized data is shown in Fig. B 3 in Appendix B.

5. Use of Eq. 8 for a linear least-squares fit to obtain the ' best ' values for A_0 and A_1. The coefficients are calculated by minimizing

$$\sum w(i) \ [Y(i) - A_0 + A_1 X(i) \ ]^2 = min \quad , \tag{9}$$

where the summation is performed over all channels i within the fitting regions below and above the edge. The weight w(i) was chosen to

$$w(i) = YNET_S(i) \cdot \ [\ell n \, 1 / T(i) \ ]^2 \quad , \tag{10}$$

neglecting the counting errors of the reference spectrum, which are $< 0.1\%$ in the fitting regions.

6. Calculation of the ratio of transmissions across the edge from Eq. 8, using the obtained values for the coefficients A_0 and A_1.
First, the ratio of transmissions is calculated for the energies E_- and E_+ at the limits of the fitting regions. The actual values chosen for E_- and E_+ are 113.25 and 117.26 keV, respectively. Note from Eq. 7 that X(i) becomes zero for the energy of the window limit. Hence, using the definition for Y(i) in Eq. 6, we calculate with Eq. 8 the logarithmic ratio of transmissions at the window limits to

$$\ell n \left[T(E_-) / T(E_+) \right] = exp \, A_0(E_+) - exp \, A_0(E_-) \quad . \tag{11}$$

The coefficients $A_0(E_-) = A_0$ (113.25 keV) and $A_0(E_+) = A_0$ (117.26 keV), together with their errors obtained from the least-squares fits, are given in the protocol.
Second, the linear fits on both sides of the edge are extrapolated beyond the limits of the fitting regions to the energy E_K of the K-absorption edge to obtain the ratio of transmissions directly at the edge energy. The coefficients A_0 and A_1 are used to calculate from Eq. 8 the extrapolated values $Y(E_K)$.

3.3.5 Calculation of the Final Result

The logarithmic ratio of photon transmissions determined at the window limits of the fitting regions are used to calculate the uranium concentration from the densitometry equation given in Eq. C 7 of Appendix C :

$$\rho\,(g/\ell) = \frac{\ell n \left[T(E_-) / T(E_+) \right]}{\Delta\mu \cdot \; d} \cdot \; 1000 \;, \tag{12}$$

where $\Delta\mu = \mu(E_+) - \mu(E_-)$ denotes the difference of the mass attenuation coefficients of uranium for the energies E_+ and E_-, and d the cell length.

The value for $\Delta\mu$ in Eq. 12 represents the calibration constant in KED which, in principle, is a physical constant. From tabulations of mass attenuation coefficients we find $\Delta\mu \simeq 3.33$ cm$^2 \cdot$ g^{-1} for the energies at the window limits of the fitting regions, and $\Delta\mu \simeq 3.55$ cm$^2 \cdot$ g^{-1} for the jump directly at the K-edge energy. The effective $\Delta\mu$-values have to be determined for the actual instrument from calibration measurements on reference solutions with known uranium concentration. The calibration of a Hybrid Instrument is described in detail in Ref. 8.

A second value for the uranium concentration, evaluated from the extrapolated transmissions at the edge energy, is given in the protocol for control purposes. This value should agree within the quoted statistical measurement errors with the result evaluated from the non-extrapolated transmissions. A statistically significant difference between the two values may be taken as an indication that the matrix composition in the measured sample substantially deviates from the matrix of the reference sample. A warning then will appear in the protocol. Note that the quoted measurement error for the ' extrapolated ' value is about two times larger than the error for the ' non-extrapolated ' value. The enlarged error arises from the extrapolation of the transmission to the edge.

Three correction factors are applied to the uranium concentration calculated according to Eq. 12. One accounts for the atomic mass of uranium, one for the sample temperature, and one for the bias caused by fission products.

Atomic Mass. The KED technique, which is based on non-isotope specific interactions with atomic electrons, principally measures the *number of uranium atoms*. In order to obtain the result expressed in mass units, the effective atomic mass, and hence the isotopic composition, must be known. Therefore Eq. 12 is multiplied by an enrichment - dependent mass correction factor

$$C_{Mass} = \frac{\varepsilon \cdot \; 235.0439 + (100 - \varepsilon) \cdot \; 238.0508}{238.0288 \cdot \; 100} \;, \tag{13}$$

where $\varepsilon = {}^{235}U/U \cdot 100$ denotes the ^{235}U enrichment expressed in atom %. C_{Mass} equals unity for natural uranium ($\varepsilon = 0.7$). The uranium enrichment is requested as input parameter. If it is not known, the program takes the default value $\varepsilon = 0.7$.

Temperature. The volume concentration measured by the instrument depends on the temperature of the sample. The software for data evaluation normalizes the concentration ρ_t measured at the ambient room temperature t (°C) to a reference temperature of 25° C using the relation

$$\rho_{25} = [1 + 0.0005\,(t - 25)] \cdot \rho_t \quad . \tag{14}$$

The ambient room temperature t is requested as input parameter. It is read from a thermometer installed inside the shielded cell.

Fission Products. The presence of fission products in real dissolver solutions will cause a small negative bias to the uranium result from KED as specified below in Sect. 3.4.3. Since the instrument usually is calibrated with synthetic solutions, an average bias correction of 0.15 % is made to the KED result whenever the instrument recognizes the presence of fission products. The information about the presence of fission products is obtained from the XRF spectrum, because the KED detector - due to the tight beam collimation - hardly detects radiations from fission products.

The total uncertainty finally assigned to the KED result for uranium will be specified below in Sect. 3.4.11 after the following discussion of the various error components for KED.

If the density of the solution is known and has been entered by the operator, the protocol also gives the concentration in units of g/kg in addition to the volume concentration.

3.4 Assessment of Error Components

In this section we give a brief account of items which actually or potentially contribute to the overall uncertainty of the KED measurement.

3.4.1 Counting Precision

Differentiating the densitometry equation (12) for the ratio of transmissions T(E.) / T(E_+) = R yields for the uncertainty of the uranium concentration

$$\frac{\Delta\rho}{\rho} = \frac{1}{\Delta\mu \cdot \rho \cdot d} \cdot \frac{\Delta R}{R} \quad , \tag{15}$$

where the uncertainty of the ratio of transmissions, $\Delta R/R$, both depends on the counting statistics and on the procedure adopted for the evaluation of the transmission ratio from the spectral data. Note from Eq. 15 that $\Delta R/R$ is multiplied by a factor inversely proportional to the concentration.

Table 1: Measurement precision for different uranium concentrations.
Basis: Counting time 1000 s live, cell length d = 2 cm, $\Delta\mu = 3.33\ cm^2 \cdot g^{-1}$

$\rho\ (g/\ell)$	$\frac{1}{\Delta\mu\rho d}$	$\frac{\Delta R}{R}$ (%)	$\frac{\Delta\rho}{\rho}$ (%)
20	7.54	0.140	1.08
50	3.02	0.156	0.472
100	1.51	0.189	0.285
150	1.01	0.229	0.231
200	0.76	0.279	0.212
250	0.60	0.350	0.210
300	0.50	0.432	0.216

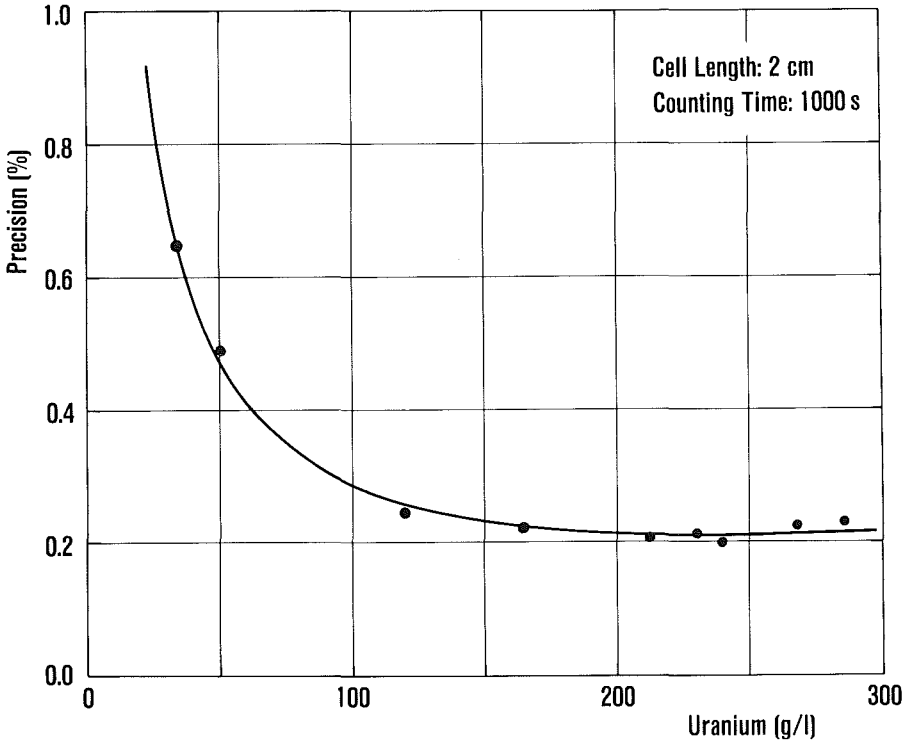

Fig. 15 : Counting precision of KED as a function of uranium concentration for a counting time of 1000 s and a cell length of 2 cm.

The uncertainty $\Delta\rho/\rho$ due to counting statistics can be calculated for the actual measurement conditions of the instrument. Table 1 gives for a set of uranium concentrations the expected counting precision $\Delta\rho/\rho$, based on a counting time of 1000 s live and a cell length d = 2 cm. The data refer to the case where the ratio of transmissions, R, is evaluated for the energies at the limits of the fitting regions (' non-extrapolated ' case). For the ' extrapolated ' case the values $\Delta R/R$ are about twice as large. Note from the table that the uncertainty of the measured ratio of transmissions, $\Delta R/R$, decreases with decreasing concentration, but that the uncertainty $\Delta\rho/\rho$ nevertheless increases due to the rapidly increasing factor $(\Delta\mu\rho d)^{-1}$. The use of a longer cell would improve the precision at lower concentrations.

The predicted measurement precision due to counting statistics is plotted in Fig. 15 as a function of the uranium concentration. Note that the precision remains fairly constant at a level of about 0.22 % for the concentration range from about 150 to 300 g/ℓ. The data points represent actually measured precision values, which are in accordance with the calculated curve.

3.4.2 Sample Dimension and Positioning

The measured concentration ρ is inversely proportional to the path length d of the X-ray beam through the solution. Thus, any uncertainty of d proportionally propagates into ρ.

The internal depth of the glass cuvettes used for KED in the Hybrid Instrument is known to 0.01%, which represents a negligible source of error. Since the dimensional variations for cuvettes from a single production batch are fairly small, it appears acceptable to use their mean value for the calculation of ρ. The mean value of the cell length and its standard deviation for the first set of 256 cuvettes was determined to d = 20.0529 cm $\pm$ 0.044%. This value is presently used as default value for d. Note that this figure eventually needs to be adjusted if lateron cuvettes from another production batch will be used.

The effective path length also depends on the position of the cell relative to the beam axis. Tilting the cuvette as shown in Fig. 16 will increase the effective path length by the factor $1/\cos\alpha$. From the machining tolerances for the sample holder we expect a maximum possible misalignment of about 2°, which will increase the path length by less than 0.1%. Note that misaligning the cuvette will cause a positive measurement bias.

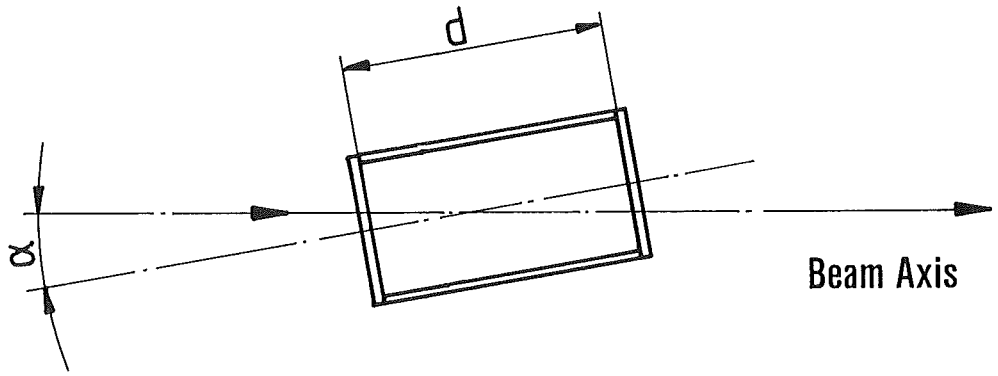

Fig. 16 : Misalignment of the glass cuvette relative to the beam axis.

3.4.3 Chemical Composition of the Sample

The general densitometry equation C 5 derived in Appendix C contains a matrix term, which cannot be neglected in those cases where the matrix composition of the measured sample substantially differs from that of the reference sample used for the acquisition of the reference spectrum. Neglecting the matrix term will cause a negative bias if the matrix of the sample contains additional elements. The magnitude of the bias depends on the concentration and atomic number of the additional matrix elements.

Fig. 17 shows the expected measurement bias for the determination of uranium in input solutions, calculated under the assumption that the instrument had been calibrated with pure nitric uranium solutions. The figure also shows how the major components of the additional matrix elements - light and heavy fission products and plutonium - contribute to the total bias as a function of the burnup. The typical concentrations of these matrix elements are given in Appendix G for a burnup of 40 GWd/t.

Note that the influence of matrix elements, as long as they are known, can be calculated from physical data. In this way the calibration constant can accordingly be adjusted for the effect of matrix elements, which reduces their impact on the uranium assay to negligible error levels.

3.4.4 Self-Radiation

In the energy region of interest the intensity of the transmitted X-ray beam for KED is about 3 orders of magnitude higher than that obtained from the self-radiation of typical input solutions. This is illustrated in Fig. 18 for an input solution from spent fuel with a burnup of 35 GWd/t and a cooling time of 3 years.

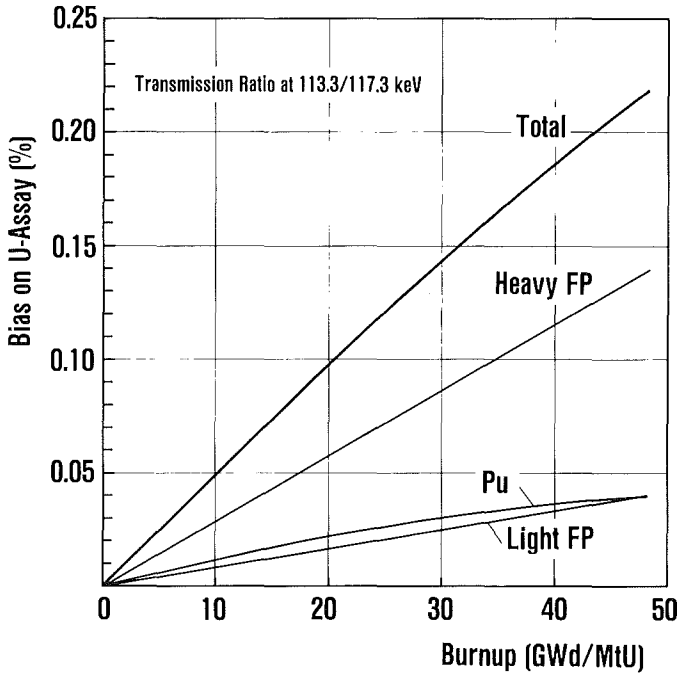

Fig. 17 : Magnitude of matrix effects on the uranium assay in input solutions.

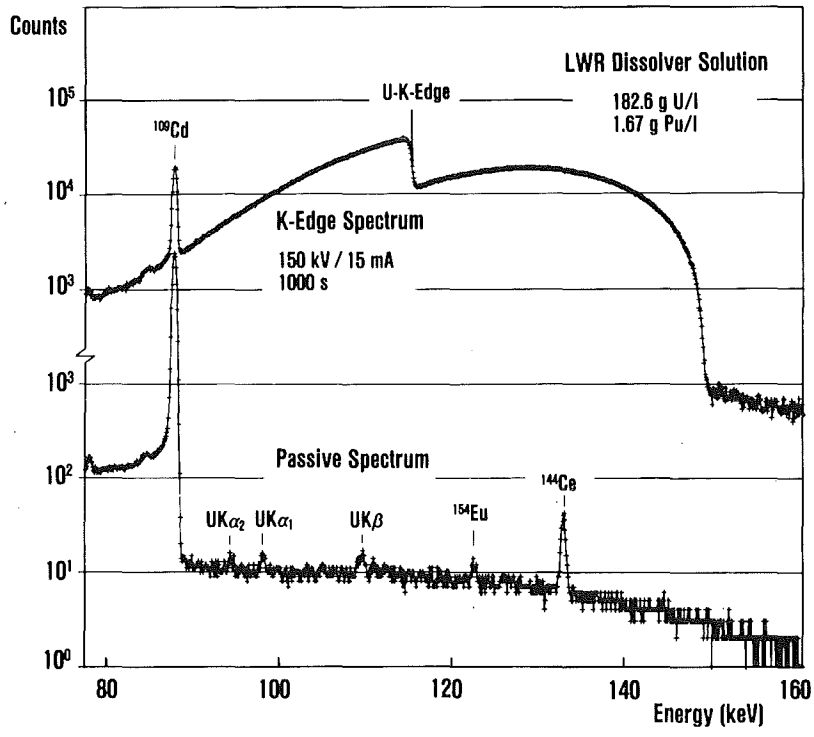

Fig. 18 : X-ray transmission spectrum (top) and spectrum of the self-radiation (bottom) measured with the K-edge detector from an input solution.

In view of this measurement situation we can safely state that KED is insensitive to the self-radiation from input solutions. This statement even holds for fuels with relatively short cooling times.

3.4.5 Uranium Isotopic Composition

The instrument calibration is based on the isotopic composition of natural uranium (see Sect. 3.3.5). If the ^{235}U enrichment in the measured sample - requested as an operator input - is not known, the calculation of the final result assumes natural enrichment. The associated bias then calculates to 0.0125% per percent enrichment deviation from natural enrichment. This is negligibly small in view of the fact that in spent LWR fuels we reasonably do not expect enrichments higher than 2 to 3%.

3.4.6 Sample Temperature

The sample temperature is needed as operator input for the normalization of the final result to a reference temperature of 25° C (see Sect. 3.3.5). If the entered temperature is not correct, the normalized result will be biased by 0.05% per ° C deviation.

3.4.7 Counting Rate

The measured ratio of photon transmissions across the K-edge is sensitive to spectral distortions such as peak tailings and pileup effects, which usually occur at higher counting rates. Significant biases of up to a few percent have been observed when samples with high concentrations were measured at high counting rates /9/. If present, these biases will also lead to a nonlinearity in the measured logarithmic ratio of the transmissions versus the concentration.

The magnitude of the potential measurement bias due to counting rate effects cannot be quantified in generally valid figures. It critically depends on specific properties of the detector and of the pulse processing system. A very sensitive parameter, for example, is the proper adjustment of the main amplifier for pole zero cancellation.

The best way to avoid this kind of potential measurement bias is to limit the counting rates for KED measurements at higher concentrations to values below about 20 kcps. This condition is met by the instrument at La Hague (see Fig. 13 in Sect. 3.2). Based on experiences with previous instruments we conclude that in the present set-up a measurement bias due to counting rate effects can reasonably be excluded.

3.4.8 Calibration Constant

With proper instrument design, the proper choice of measurement conditions, and the correct determination of the ratio of transmissions across the

K-edge we expect that the densitometry equation holds. Under this assumption a single constant ($\Delta\mu$) has to be determined for calibration.

The error of the calibration constant is determined by two components: an internal component associated with the KED measurements, and an external component given by the uncertainty of the chemical reference values for the calibration solutions. In the calibration exercise described in Ref. 8 the internal component was determined to 0.04%, which was far less than the error of the chemical reference values.

In Section 3.4.3 it was shown that the instrument response for uranium in an input solution can be well predicted in relation to the response from a pure uranium solution. Hence, it is possible to base the calibration for input solutions on synthetically prepared pure uranium solutions. It is assumed that the reference concentrations for those solutions can be determined to 0.1% by chemical assays. Ultimately, this figure will determine the lower limit of the calibration error for KED.

3.4.9 Instrument Variability

The instrument response for KED can slightly vary with time due to unpredictable variabilities of relevant instrument components. The short- and long-term behaviour is best monitored from regular control measurements on specially prepared reference samples.

The fact that KED is based on a *ratio measurement* greatly reduces drifts of the instrument response. Experiences with existing K-edge densitometers have shown that long-term drifts are usually in the range of $\leq$ 0.3%. Fig. 19 shows the behaviour of the KED response of the present instrument as it is known so far. The results of about 50 control measurements performed on the sealed uranium reference solution during a period of 6 months indicate long-term drifts of 0.3 % at maximum.

3.4.10 Summary of Error Components for KED

For a quick survey Table 2 summarizes the various error components and their estimated magnitude, as they are expected for the KED measurement in the Hybrid Instrument at La Hague.

3.4.11 Uncertainty Assigned to the KED Result

The total uncertainty presently assigned to the KED result for the uranium concentration takes into account the following error contributions :

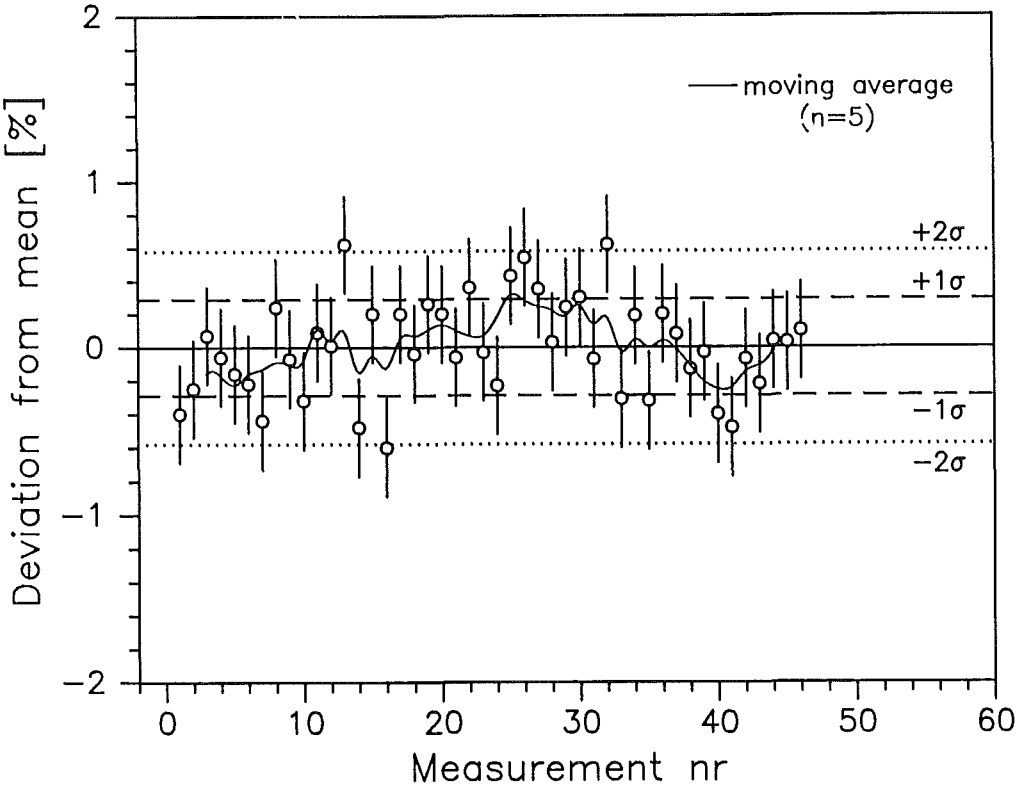

Fig. 19 : Results of control mesurements for KED performed on the sealed uranium solution during a period of 6 months.

- *Counting precision*: Taken as precision $\sigma = [(1/n)\cdot \Sigma^n \sigma_i] / \sqrt{n}$ for the mean value of n repeat measurements with individual precision σ_i. The standard procedure normally includes 3 repeat runs at 1000 s each;
- *Calibration error:* 0.1 %;
- *Cell length and positioning:* 0.1 %;
- *Concentration of fission products*: 0.05 %. This error accounts for the uncertainty of the average bias correction of 0.15 % for fission products mentioned in Sect. 3.3.5, if the burnup of the fuel is not known. A bias correction of 0.15 ± 0.05% holds for the burnup range of 32 ± 12 GWd/t;
- *Instrument variability*: A preliminary error of 0.2 % is taken until a realistic magnitude of this component can be deduced from an enlarged set of control measurements performed with the present instrument for a longer period.

The above independent error components, if quadratically added up, lead to a total uncertainty of 0.25 to 0.30 % at the 1σ- level for uranium concentrations between about 100 and 300 g/ℓ.

Table 2 : Summary of Error Sources for KED

Error Source	Magnitude of Error (%)	Remark
Counting precision	0.15	150 - 300 g U/ℓ. Counting time 1 h
Cell length	0.01 <0.1	For individual cuvette. Variation for a production batch of cuvettes
Positioning of cell	<0.1	Determined by dimensional tolerances for sample holder
Sample matrix	<0.2	Effect calculable. Can be taken into account in calibration
Uranium isotopic comp.	0.013	Per % change of ^{235}U enrichment
Sample temperature	0.05	Per °C change of sample temperature
Calibration	0.1	Determined by error of chemical reference values
Nonlinearity	<0.2	For counting rates <20 kcps at concentrations ≥ 200 g/ℓ
Instrument variability	<0.3	To be monitored from control charts

4. X - Ray Fluorescence Measurement

The primary information obtained from the XRF measurement on dissolver solutions is the *U/Pu ratio*, which is derived from the ratio of the measured net peak area of the $UK\alpha_1$ and $PuK\alpha_1$ X-rays. The U/Pu ratio is then combined with the uranium concentration determined by the parallel KED measurement to calculate the value for the plutonium concentration. Note that in this way the XRF analysis for dissolver solutions is only used to measure a *ratio* but not *absolute* concentrations. The discussions in this chapter will concentrate on this mode of analysis.

However, the XRF branch of the Hybrid Instrument can also be used as a stand-alone technique to obtain absolute concentrations. This mode is occasionally required to measure process samples of lower concentrations ($\leqq$ 20 g/l), for which KED no longer provides sufficient measurement precision. This mode will be briefly discussed in Sect. 4.5.

4.1 Features of the XRF Spectrum

The top spectrum in Fig. 20 displays a typical XRF spectrum from a dissolver solution. It features a broad 'bump' in the middle portion, superimposed with characteristic X-rays from uranium and plutonium. Some spurious X-rays from tungsten, excited in the materials for collimation and shielding, are also visible. The physical processes leading to the emission of characteristic X-rays are briefly described in Appendix D. This Appendix also lists the energies and relative abundances of K-series X-rays from uranium and plutonium.

The XRF spectrum, accumulated into 2K channels and covering radiations up to about 150 keV, also contains some gamma rays from longer-lived fission products such as ^{144}Ce, ^{154}Eu and ^{155}Eu. The self-radiation of the sample is better seen from the passive spectrum (bottom spectrum in Fig. 20), which was accumulated with the X-ray tube switched off. The self-radiation of the input solution also shows X-rays from uranium and plutonium, which are excited by the intense radiation of the fission products. These internally excited X-rays usually contribute less than 0.5% to the X-ray intensity generated by the X-ray beam from the tube.

The broad ' bump ' of counts in the middle portion of the XRF spectrum is due to the inelastic scattering of the primary X-ray beam, which preferably takes place at the low-atomic-number elements (H, N, O) of the liquid sample. The

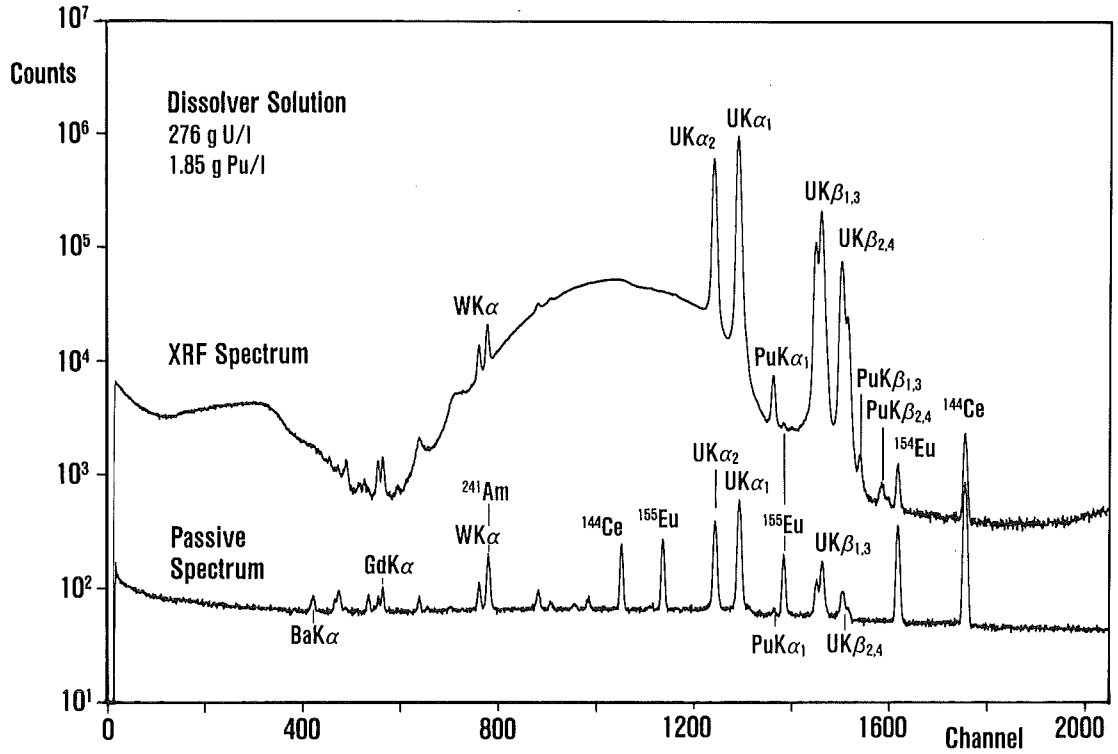

Fig. 20 : Typical XRF spectrum (top) and passive spectrum (bottom) measured with the XRF detector from an input solution.

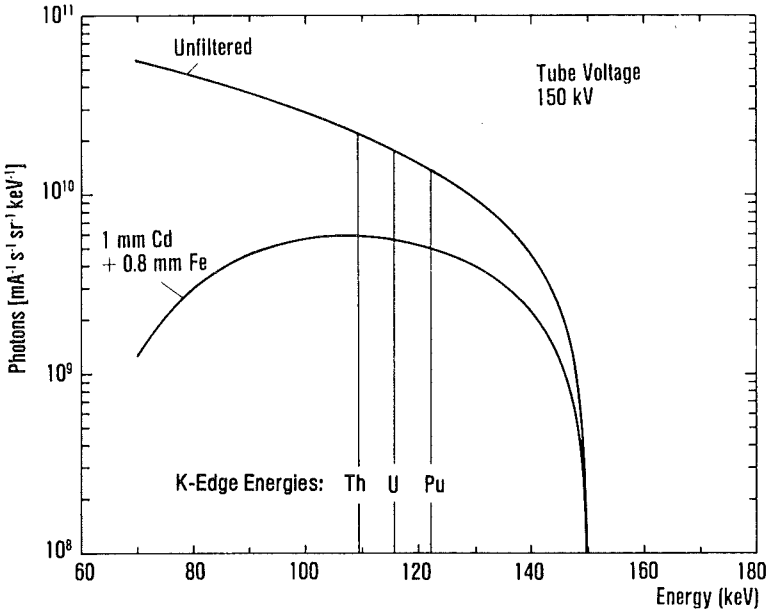

Fig. 21 : Spectral distribution of the filtered X-ray beam used for XRF (bottom curve).

bottom curve in Fig. 21 shows the spectral distribution of the filtered primary X-ray beam irradiating the PE vial for XRF. A large fraction of these X-rays becomes inelastically scattered with degraded energy towards the XRF detector. For the Hybrid Instrument, realizing an angle $\theta = 150°$ between the incident and scattered beam direction (see Fig. 2 in Sect. 2.1), the energy loss is about 55 keV for the maximum incident photon energy of 150 keV, as explained in Appendix F. In this way most of the scattered radiation becomes removed from the region where the uranium and plutonium K X-rays occur. However, there remains the situation that more than 50% of the total recorded counts in the XRF detector represent useless scattered radiation.

4.2 Counting Rate

The beam collimation in front of the XRF detector was adjusted to keep the total counting rate below 40 kcps. The counting rate does not significantly change as a function of the uranium concentration (see Fig. 13 in Sect. 3.2). For an input rate of 35 kcps the system dead-time is about 30%. Therefore the preset live-time of 1000 s for a single XRF run actually corresponds to a real measurement time of about 1450 s.

4.3 Spectrum Analysis

4.3.1 Evaluation of Spectral Data

The U/Pu weight ratio is derived from the measured net peak area ratio of the fluoresced $UK\alpha_1$ and $PuK\alpha_1$ through the relation

$$\frac{U}{Pu} = \frac{A(U)}{A(Pu)} \cdot \frac{P(UK\alpha_1)}{P(PuK\alpha_1)} \cdot \frac{ORE(PuK\alpha_1)}{ORE(UK\alpha_1)} \cdot \frac{1}{R_{U/Pu}} \qquad (16)$$

with

A = atomic weight for uranium and plutonium, respectively,
P = net peak area of the $K\alpha_1$ X-rays
ORE = overall relative detection efficiency for the $K\alpha_1$ X-rays,
$R_{U/Pu}$ = calibration factor describing the ratio of excitation probabilities for emission of $UK\alpha_1$ and $PuK\alpha_1$ X-rays in the primary X-ray beam.

The quantities to be determined from the XRF spectrum are the net peak areas P, and the overall relative detection efficiency ORE for the $K\alpha_1$ lines from the two elements. The software for spectrum analysis includes the following steps:

1. Energy calibration, using the uranium X-rays at 94.66 keV ($UK\alpha_2$) and 111.30 keV ($UK\beta_1$) as reference lines. The peak positions are determined in the same manner as in the software for KED.

2. Subtraction of the background in the spectral regions including the $UK\alpha_2$, $UK\alpha_1$ and the $UK\beta$ X-rays. For this a smoothed step function is calculated between the average background levels determined from background windows set on either side of the respective peak groups as indicated in Fig. 22. The smoothed step-like background is calculated using Eq. 1 given in Section 3.3.2.

3. Subtraction of the background below the $PuK\alpha_1$ line, which is taken in proportion to the sum of the counts in background windows centered 1.7 keV below and 3.7 keV above the peak position. The proportionality factor, given as 'Bkg-Calib. Factor' in the protocol, has been established from calibration measurements. Another window is set at the energy of the $AmK\alpha_1$ X-ray. The counts from this window are used to correct for possible interferences of the $AmK\alpha_2$ line to the background window below the $PuK\alpha_1$ line, and to provide an estimate for the concentration of Am, if present.

4. Subtraction of the background level from the self-radiation of an input sample below all X-ray peaks. The respective background is taken in proportion to the additional counts observed in the spectral region between the fission product gamma rays from ^{154}Eu (123.07 keV) and ^{144}Ce (133.54 keV). The peak area of the ^{154}Eu line at 123.07 keV is also determined and used as a criteria for an eventual bias correction to the KED result for uranium.

5. Determination of the energy resolution (*FWHM*) as a function of energy. The *FWHM*-values determined from a Gaussian fit to the $UK\alpha_2$, $UK\alpha_1$ and $UK\beta_1$ X-rays are used as input to a linear least-squares fit of the form ($FWHM^2$ - 0.46 $GAIN^2$) versus *ENERGY* /7/. The additional line broadening of the X-rays due to their intrinsic natural width is taken into account.

6. Calculation of the net peak counts from a summation of the background-corrected counts within a peak region of $\pm$ 1.1 *FWHM* relative to the peak maximum. For the $UK\beta_{1,3}$ complex the summation extends from $E(UK\beta_3)$ - 1.1 *FWHM* to $E(UK\beta_1)$ +1.1 *FWHM*. The peak counts of the $UK\alpha_1$ line are corrected for the interference from the adjacent $PuK\alpha_2$ X-ray.

7. Calculation of the overall relative detection efficiency *ORE* between 94.66 keV ($UK\alpha_2$) and 111.30 keV ($UK\beta_1$), using the measured net peak areas of the uranium K X-rays $UK\alpha_2$, $UK\alpha_1$ and $UK\beta_{1,3}$ together with their known relative emission probabilities as input to a linear least-squares fit of *ORE* versus *ENERGY*.

4.3.2 Calculation of Final Results

The measured net peak areas and relative detection efficiencies are used to calculate the U/Pu weight ratio according to Eq. 16. The calculation of this ratio requires the following additional data:

- The atomic weights *A(U)* and *A(Pu)* for the actual uranium and plutonium in the sample. *A(U)* is obtained as input data from the parallel KED measurement. If *A(U)* is not known, the program for data evaluation takes the atomic weight of natural uranium as default value. For *A(Pu)* a fixed value of 239.6333 is taken, which reasonably approximates the atomic weight of plutonium from spent LWR fuels (see Section 4.4.3).
- The calibration factor $R_{U/Pu}$, which according to the calibration measurements reported in Appendix H was determined to

$$R_{U/Pu} = 1.4987 \cdot \exp - (1.10224 \cdot 10^{-4} \cdot \rho_u [g/\ell]). \qquad (17)$$

Note that for the calculation of the actual calibration factor also the uranium concentration ρ_u is required. The value for ρ_u is obtained from the parallel KED measurement.

Finally, the protocol also reports the absolute plutonium concentration in g/ℓ, which is calculated from the U/Pu ratio from the XRF measurement and from the uranium concentration as measured by KED. Further, an estimate for the Am concentration, if detected, is also given.

4.4. Assessment of Error Components

Below we list those items, which influence the total uncertainty of the XRF measurement for the U/Pu weight ratio.

4.4.1 Counting Precision

The by far dominating error component of the XRF measurement is the counting error for the $K\alpha_1$ X-ray of the minor element plutonium. Only about 0.1% of the total counts recorded in the XRF spectrum fall into the $PuK\alpha_1$ line. For a

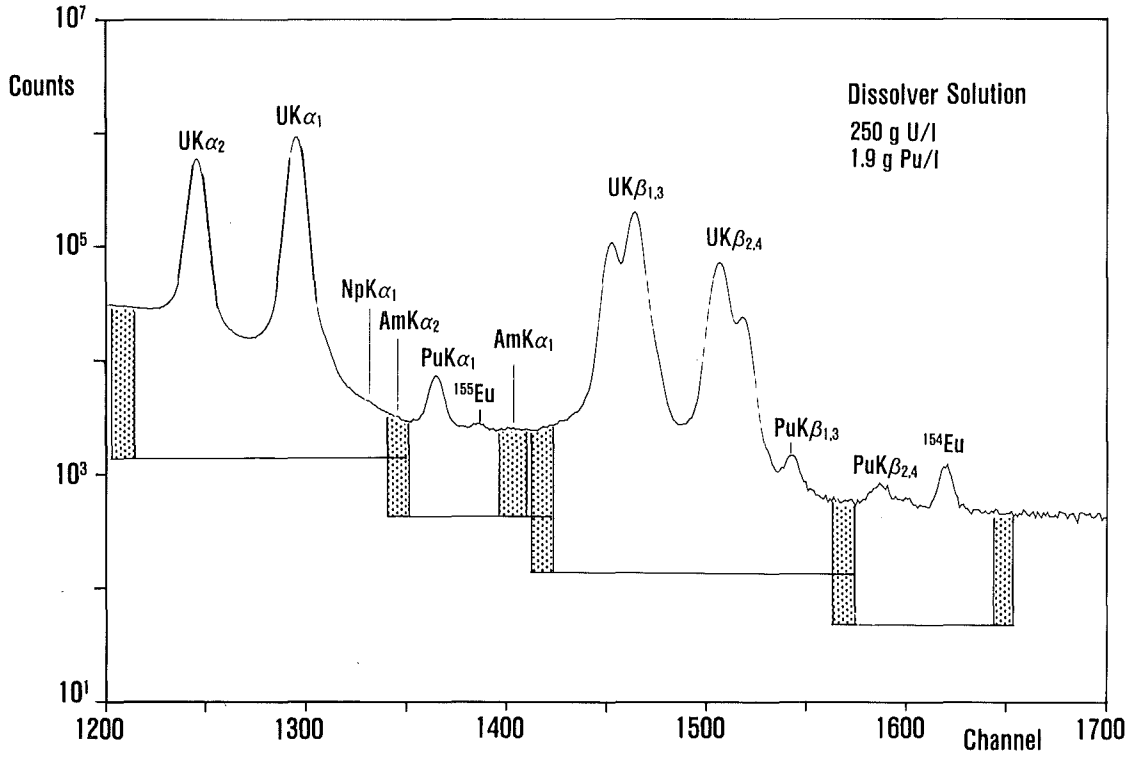

Fig. 22 : Set of background windows used for the evaluation of net X-ray peak areas from the XRF spectrum.

1000 s counting time typically about 30 000 to 50 000 net peak counts are accumulated from this X-ray. For a typical peak-to-background ratio of about 1 this yields a counting precision for plutonium as shown in Fig. 23.

The typical plutonium concentration in input solutions is about 2 g/ℓ. For this concentration the counting precision for a single 1000 s run is approximately 0.8%, and about 0.5% for the mean value of the 3 repeat runs.

4.4.2 Sample Properties

It is expected that small variations of the chemical composition and geometry of the samples for XRF will have a negligible effect on the U/Pu ratio measurement. Correct results will be obtained even with an incompletely filled vial. This has been experimentally verified. The actual concentration of the major element uranium, which slightly affects the value of the calibration factor $R_{U/Pu}$, is accordingly taken into account (see Eq. 17 in Sect. 4.3.2).

A small systematic error, if not corrected for, could eventually be introduced by the self-radiation. The spectrum of the self-radiation from an input solution exhibits, as shown in Fig. 20 in Sect. 4.1, uranium and plutonium X-rays excited by the internal radiations of the sample. In principle, these X-rays would

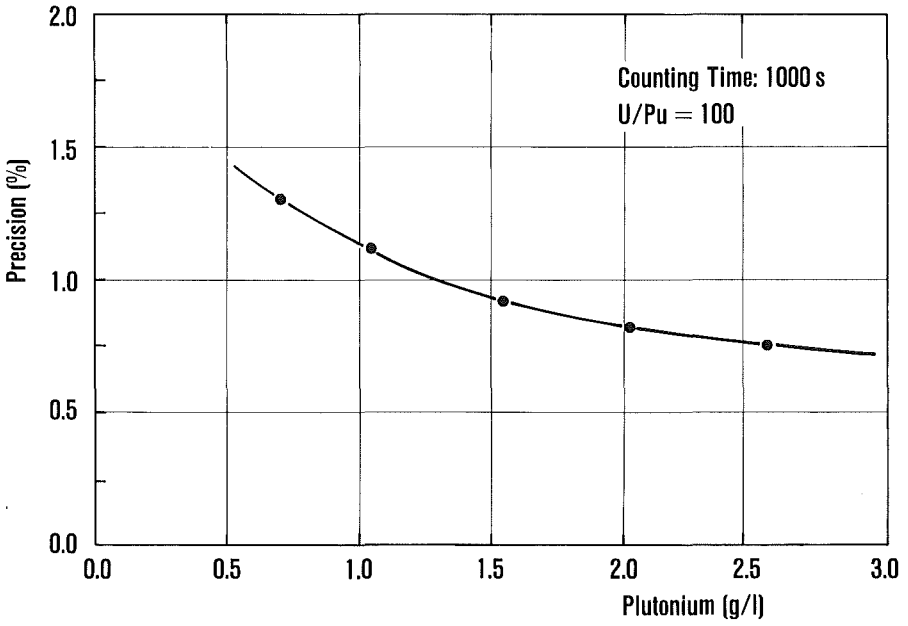

Fig. 23 : Counting precision for plutonium from the XRF measurement.

not affect the U/Pu ratio measurement as long as the ratio of uranium and plutonium X-rays generated by the internal radiations and by the incident external beam is about the same. In practice, however, this is not true, because the external beam excites uranium with about 1.5 times higher probability than plutonium, whereas the excitation probabilities for both elements due to the internal radiations are about the same.

For the present instrument at La Hague we expect a contribution from the self-radiation to the measured X-ray intensities of about 0.1-0.2% at maximum. This means that the measured intensity ratio $UK\alpha_1/PuK\alpha_1$ has to be increased by about 0.1% in order to obtain the true ratio due to external beam excitation.

The best way to control the contributions from the self-radiation is, of course, to acquire a separate passive spectrum. However, in order to avoid this additional measurement, provision has been made to derive the necessary corrections from the XRF spectrum itself. This is accomplished using relations between the additional counts from fission products observed in the region between 125 and 131 keV and the passive countrate in the windows used for the evaluation of the net X-ray peak areas. The proportionality factors for the above relations were derived from a number of different passive spectra. It is estimated that for typical ranges of burnup and cooling time the applied corrections, accounting both for the internally excited X-ray intensity and the average

additional background level, reduces the potential bias due to fission products to less than 0.3%.

4.4.3 Atomic Weights

The atomic weights *A(U)* and *A(Pu)* for uranium and plutonium are required to convert the measured U/Pu atom ratio into the U/Pu weight ratio. For *A(Pu)* a fixed value of 239.6333 is taken. This reasonably approximates the atomic weight of plutonium typically occurring in input solutions from LWR fuels. Table 3 gives the approximate isotopic composition of medium and high-burnup plutonium. It can be seen that the value chosen for *A(Pu)* well approximates the effective atomic weights for the expected range of plutonium isotopic compositions. The expected maximum deviation is $< 0.1\%$.

The atomic weight *A(U)* of uranium, if not known, introduces a negligible error contribution (see Sect. 3.4.5).

4.4.4 Instrument Variability

The stability of the high voltage applied to the X-ray tube is probably the most critical instrumental parameter for the U/Pu ratio measurement. Fig. 24 shows how the production rates for the $UK\alpha_1$ and $PuK\alpha_1$ X-rays, and their ratio, varies with the tube voltage. At the nominal voltage setting of 150 kV the ratio of generated $UK\alpha_1$ and $PuK\alpha_1$ X-rays changes by 1.1%, if the tube voltage is changed by 1 kV.

The specified voltage stability of the X-ray generator is $\pm$ 0.1%. This corresponds to an uncertainty of 0.17% for the ratio of $UK\alpha_1$ and $PuK\alpha_1$ X-rays. Because of its importance for the XRF measurement, the high-voltage for the X-ray tube is regularly monitored from the end point energy of the transmission spectrum for KED as described in Sect. 3.3.1. From the respective data we conclude that the actual voltage stability of the HV generator is at least a factor of 2 better than the specified value of $\pm$ 0.1%.

Other instrument variabilities affecting the measured U/Pu ratio should be small. As for KED we also expect for the XRF measurement, which simply determines the ratio of two X-ray intensities, that the instrument variabilities remain $\leq 0.3\%$. For the control and assessment of possible short - and long - term variabilities a special reference sample (MOX pellet) as described in Sect. 2.2.4 is provided with the instrument. This reference sample should be measured on a regular basis for the purpose of measurement control.

Table 3 : Approximate Atomic Mass of Medium and High-Burnup Plutonium

Isotope	Atomic Mass (*A*)	Approximate Abundance (%) High Burnup	Medium Burnup
238	238.0494	2	1
239	239.0521	55	70
240	240.0538	25	20
241	241.0567	12	6
242	242.0586	6	3
Atomic Mass of Mixture (*A*)		239.703	239.453
Deviation from Default Value (239.6333)		+ 0.029%	- 0.075 %

Fig. 25 displays the results of 52 control measurements on the MOX pellet obtained during the first 7 months of instrument operation. The standard deviation of 0.27% for this set of data is not significantly different from the estimated precision of 0.24% for a single measurement.

4.4.5 Calibration Factor

The standard error of the calibration factor $R_{U/Pu}$ was determined from the calibration measurements to 0.14% (see Appendix H). Together with the uncertainty of ± 0.05% of the chemical reference values for the U/Pu ratio the total error of the calibration factor is estimated to 0.15%.

4.4.6 Summary of Error Components for XRF

Table 4 summarizes for a quick survey the various error components and their estimated magnitude, as they are expected for the U/Pu determination

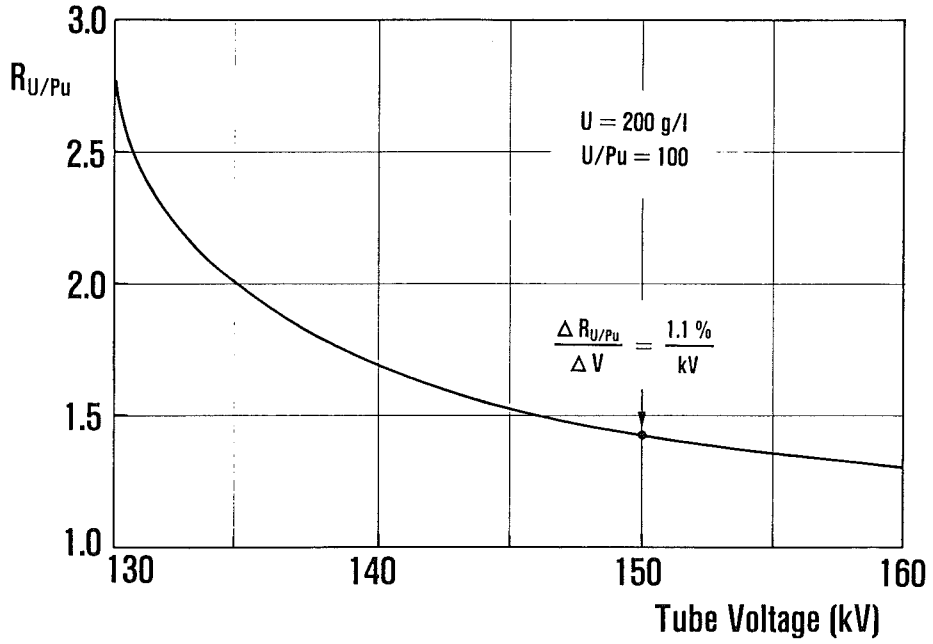

Fig. 24 : Dependence of the ratio of production rates for uranium and plutonium X-rays on the tube voltage.

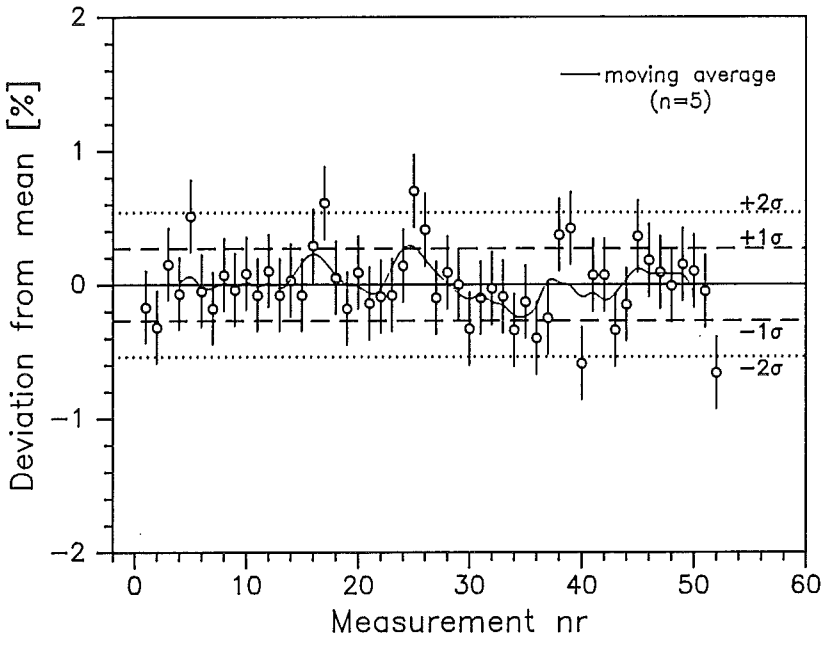

Fig. 25 : Results of XRF control measurements on the MOX pellet for the first 7 months of instrument operation.

from the XRF measurement. Note that the measurement errors for XRF and KED have to be combined when absolute plutonium concentrations are calculated from the results of both measurements.

Table 4 : Summary of Error Sources for the U/Pu Ratio Measurement from XRF

Error Source	Magnitude of Error (%)	Remark
Counting precision	0.5	For 2 g Pu/ℓ. Counting time 1 h
Self-radiation	0.3	Can be determined from a passive spectrum
Atomic weights	< 0.1	Correction with known isotopic compositions possible
Calibration factor	0.15	Depends on extent of calibration efforts
Instrument variability	< 0.3	To be monitored from control charts

4.4.7 Uncertainty Assigned to the Pu Concentration

The total uncertainty of the reported result for the plutonium concentration in an input solution combines the error of the KED measurement for uranium as stated in Sect. 3.4.11, and the error of the XRF measurement for the U/Pu ratio. The latter includes the following error components :

- *Counting precision* : Taken as precision $\sigma = [(1/n)\cdot\Sigma^n \sigma_i] / \sqrt{n}$ for the mean value of n repeat measurements with individual precision σ_i. The standard procedure normally includes 3 repeat runs at 1000 s each;

- *Calibration error* : 0.1%;

- *Correction for self-radiation from fission products* : 0.1%;

- *Instrument variability* : 0.2%.

The different error components, if quadratically added up, yield a total uncertainty of about 0.7% at the 1σ-level for typical plutonium concentrations (2 g/ℓ) in dissolver solutions. This uncertainty is based on a counting time of 1 h.

4.5 XRF for Low Concentrations

Process samples in which both the uranium and plutonium concentration is below about 20 g/ℓ are measured by XRF alone. Typical XRF spectra taken from solutions containing uranium and plutonium at a concentration of 1 g/ℓ are shown in Fig. 26.

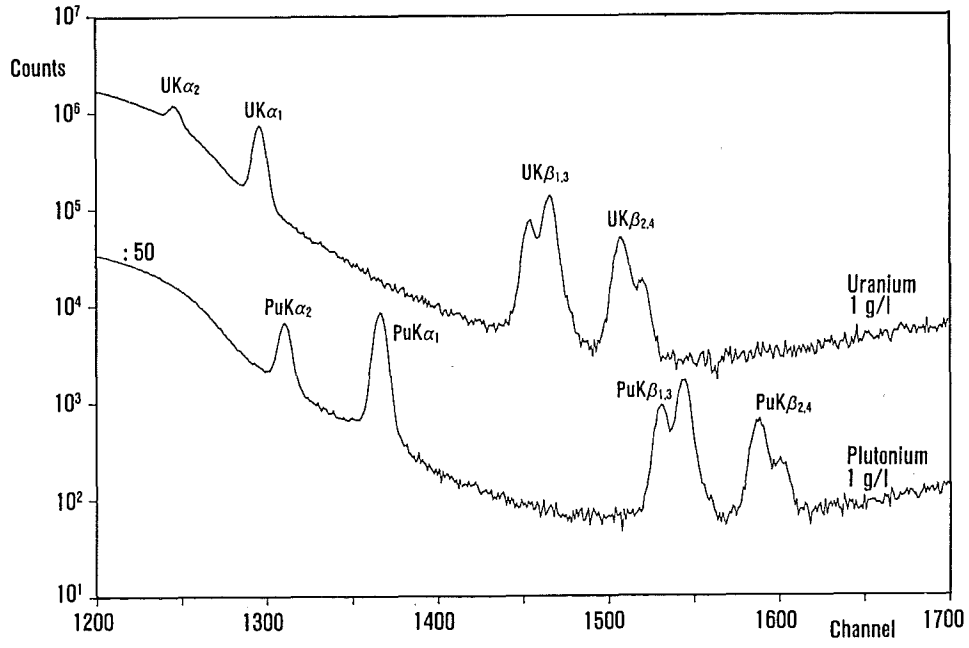

Fig. 26 : XRF spectra from solutions containing uranium (top) and plutonium (bottom) at 1 g/ℓ.

The concentration of uranium is determined from the intensity of its $K_{\beta 1,3}$ line. This X-ray, though being less intense than the $K_{\alpha 1}$ line, allows a more accurate peak area determination because of its favorable peak-to-background ratio. For plutonium, however, the $K_{\alpha 1}$ line represents the better choice for analysis. Fig. 27 shows the measurement precision for both elements as a function

of concentration obtained within a counting time of 1000 s. For this measurement time the limit of detection at the 3σ-level is 8 mg/ℓ for both elements.

The relationship between the measured net peak area of the respective X-rays and the element concentration has been established from calibration measurements on reference solutions. For concentrations up to about 10 g/l the calibration curve turns out to be nearly linear. Since the photon output of the X-ray tube can fluctuate by about ± 1%, provision has been made to monitor the intensity of the incident X-ray beam. This is accomplished by measuring the intensity of the straight-through beam with the KED detector. For this purpose an additional beam filter of 2 mm of cadmium, inserted by means of a sleeve into a slot next to the KED detector, is required to reduce the detector counting rate to a level of about 20 kcps. The integrated counts in the energy bin between the K-absorption edge energy of uranium and the endpoint energy of the X-ray continuum are used as reference for normalization.

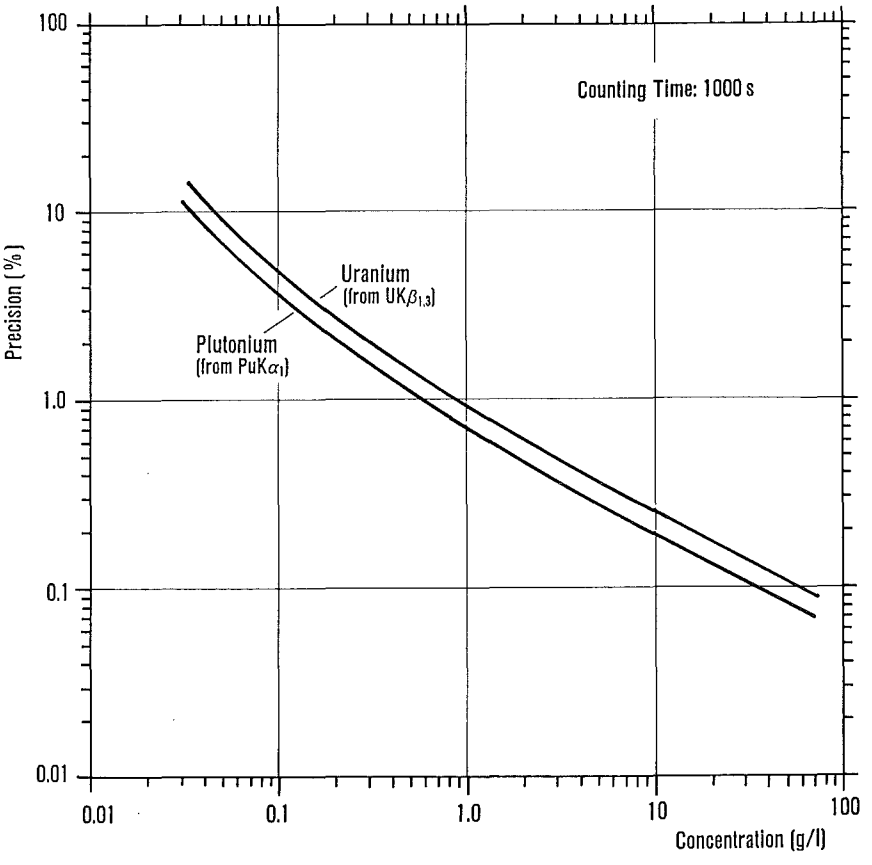

Fig. 27 : Counting precision for the determination of uranium and plutonium from an XRF measurement of 1000s.

5. References

/1/ H. Ottmar, ESARDA Bulletin No. 4 (April 1983)

/2/ H. Ottmar, H. Eberle, P. Matussek, I. Michel-Piper, Report KfK 4012 (1986)

/3/ H. Ottmar, H. Eberle, L. Koch, Journal INMM Vol. XV (1986) 632

/4/ J.F. Gueugnon, K. Richter, Note Technique K 0289127, European Institute for Transuranium Elements, Karlsruhe

/5/ H.P. Weise, P. Jost, W. Freundt, Proc. 1st European Conf. on Non - Destructive Testing, Mainz, April 24-26 (1978) p. 23

/6/ E. Storm, H. Israel, Nuclear Data Tables 7 (1970) 565

/7/ R. Gunnink, W.D. Ruther, Report UCRL - 52917 (1980)

/8/ H. Ottmar, H. Eberle, I. Michel-Piper, E. Kuhn, S. Johnson, Report JOPAG / 11.85 - PRG - 123, Kernforschungszentrum Karlsruhe (1985)

/9/ H. Eberle, P. Matussek, I. Michel-Piper, H. Ottmar, Proc. 9th ESARDA Symp. on Safeguards and Nucl. Mat. Manag., London, U.K. 12- 14 May, 1987, EUR 11041 EN, ESARDA 21 (1987) 179; Report KfK 4291 (1987)

/10/ H. Ottmar, H. Eberle, P. Matussek, I. Michel-Piper, Advances in X-Ray Analysis 30 (1987) 285

/11/ D.C. Camp, W.D. Ruther, Report UCRL-51883 (1979)

/12/ M.C. Edelson, in ' Inductively Coupled Plasma in Analytical Atomic Spectrometry ', Chapter 7, edited by A. Montaserand and D.W. Golightly (1987)

/13/ Philips GmbH, private communication

/14/ U. Fischer, H.W. Wiese, Report KfK 3014 (1983)

Appendix A. **Types of Photon Interactions with Matter**

Fig. A 1 illustrates the various processes which occur when X-ray photons (or generally photons) impinge on matter. For the range of photon energies prevailing in the Hybrid Instrument ($E \leq 150$ keV) there exist four possibilities :

(i) *Transmission.* The photon passes the matter without any interaction.

(ii) *Absorption.* The photon undergoes a so-called photoelectric interaction. It transfers its complete energy to a bound atomic electron and disappears.

(iii) *Inelastic Scattering.* The photon becomes scattered from atomic electrons. It changes its direction and looses some of its energy.

(iv) *Elastic Scattering.* The photon becomes scattered from atomic electrons. It changes its direction but not its energy.

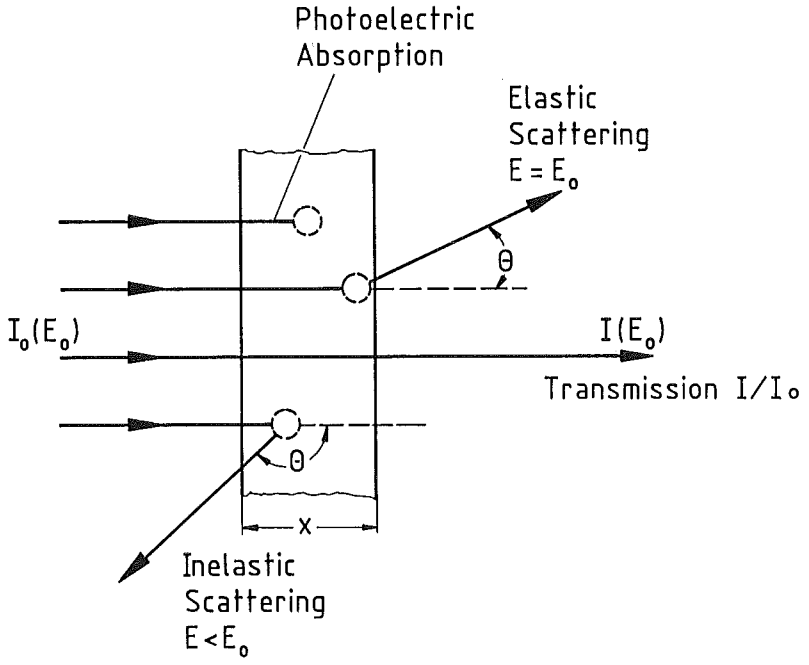

Fig. A 1 : Interactions of photons with matter.

The relative importance of the different processes depends on the energy of the incident radiation, and on the atomic-number of the elements present in the matter. Fig. A 2 shows for a low-atomic number element (oxygen, $Z = 8$) and for a high-atomic-number element (uranium, $Z = 92$) the coefficients for photoelectric interaction (τ), inelastic scattering (σ_{inel}), elastic scattering (σ_{el}), and for the sum $\mu = \tau + \sigma_{inel} + \sigma_{el}$ as a function of incident photon energy. The coefficients are expressed in units of $cm^2 \cdot g^{-1}$. μ is called the *mass attenuation coefficient.*

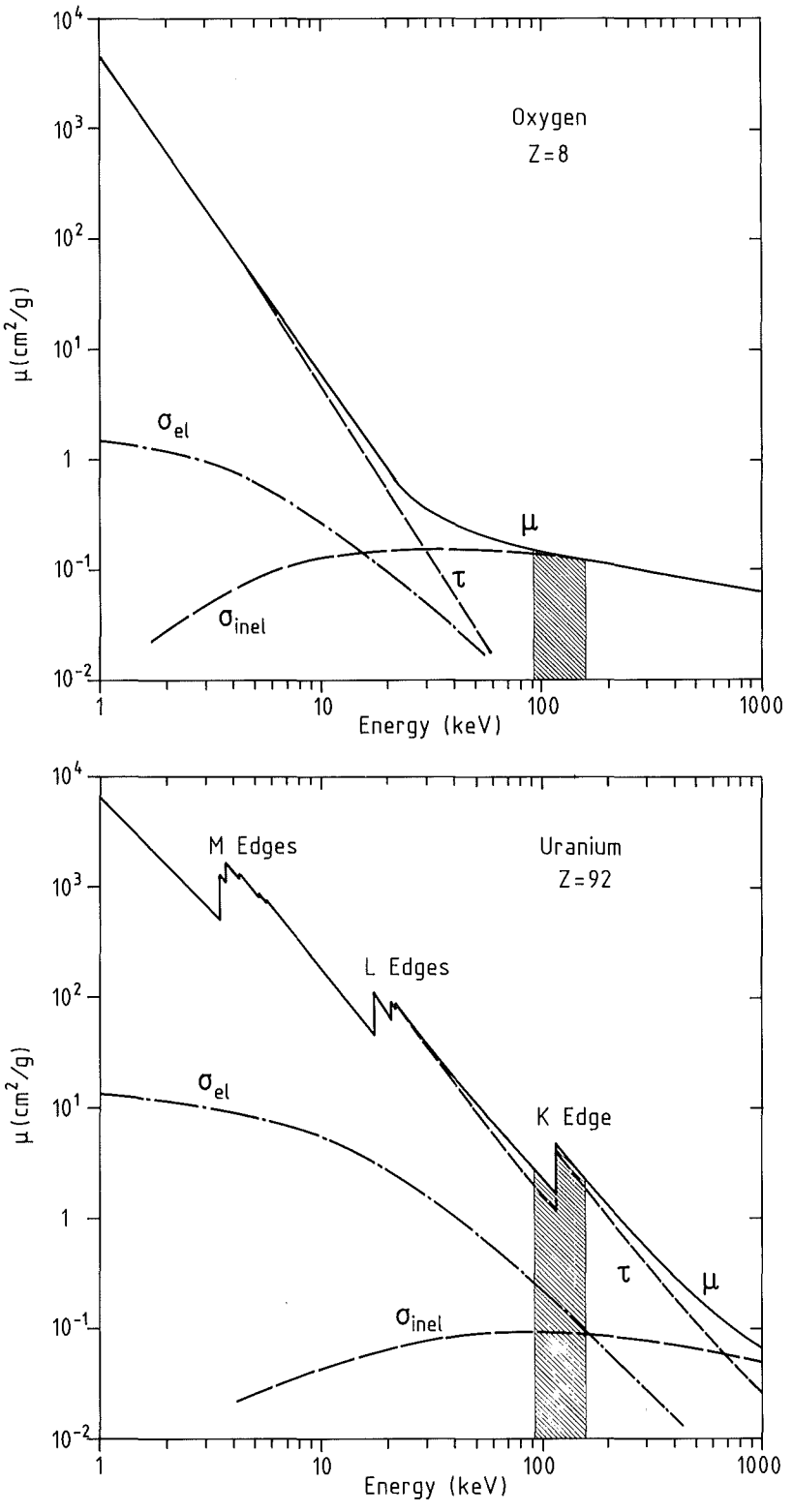

Fig. A 2 : Mass attenuation coefficient and its components for oxygen (top) and for uranium (bottom) as a function of incident photon energy.

Note from the figure that for photon energies prevailing in the Hybrid Instrument - indicated by hatched areas - the dominating process for low-atomic-number elements is inelastic scattering, whereas for high-atomic-number elements the photoelectric interaction dominates. Further note that the photoelectric coefficient, τ, and hence the total mass attenuation coefficient, μ, shows discontinuities at characteristic energies (for oxygen the absorption edge of highest energy occurs at 0.54 keV, which is outside the scale of the figure). The energy of this so-called absorption edges corresponds to the electron binding energy in the respective atomic shell (K, L, M, . . .) of the given element. Whenever the energy of the incident photon exceeds the binding energy of an electron in its shell, a photoelectric interaction with this electron becomes possible, leading to an abrupt increase of the coefficients τ and μ.

Table A 1 : Electron Binding Energy (keV) in the K-Shell and L-Subshells /6/.

Element	Atomic Number	K	L_I	L_{II}	L_{III}
H	1	0.014			
O	8	0.533	0.024	0.009	0.009
Ge	32	11.104	1.413	1.248	1.217
Er	68	57.486	9.752	9.264	8.358
U	92	115.606	21.759	20.948	17.170
Pu	94	121.797	23.109	22.270	18.063

The electron binding energies in atomic shells - and hence the absorption edge energies - are characteristic for a given atomic number Z. Table A 1 lists for a few elements the electron binding energies for the 4 innermost atomic shells (K, L_I, L_{II}, L_{III}). The binding energy increases with the atomic number Z. Note, for example, that for a K-shell photoelectric effect in U and Pu the incident radiation must have an energy >115.6 keV for U, and $>$ 121.8 keV for Pu.

The discontinuity of the mass attenuation coefficient at the element - specific K - absorption edge forms the basis of K-edge densitometry. The change of μ across a given edge, $\Delta\mu$, takes characteristic values for each element. We have determined the K-edge jump $\Delta\mu_K$ for U and Pu to 3.546 and 3.272 $cm^2 \cdot g^{-1}$, respectively /10/.

Appendix B. **Photon Transmission**

In Fig. B 1 an X-ray beam of intensity I_0 (E) photons per second strikes a differential slab dx of material perpendicular to the surface. The energy of each incident photon is E. The rate of photons which is transmitted through the slab without interacting with the material is I_0 (E) - dI (E).

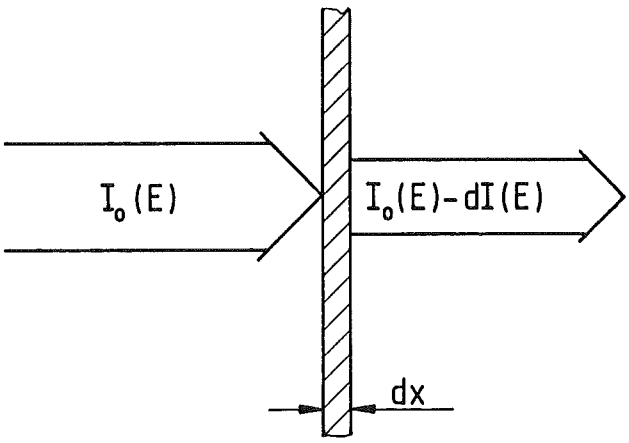

Fig. B 1 :

Photon Transmission

The number of photons which interacted in the slab, - dI(E), is expected to be proportional to both the incident photon rate I_0 (E) and the mass per unit area of the slab, which is given by $\rho \cdot dx$:

$$- dI(E) = \mu(E) \cdot I_o(E) \cdot \rho \cdot dx \quad . \tag{B 1}$$

The proportionality constant is the mass attenuation coefficient μ(E). For a piece of material of finite thickness d, integration of Eq. B 1 yields

$$I(E) = I_o(E) \cdot e^{-\mu(E)\,\rho\,d} \quad . \tag{B 2}$$

The ratio of transmitted to incident photon rate,

$$T = I(E) / I_o(E) = e^{-\mu(E)\rho\,d} \tag{B 3}$$

is called *transmission*. Note that in the vicinity of an absorption edge, where μ(E) shows a discontinuity, also the transmission exhibits a discontinuity.

If the substance contains i elements, the effective mass attenuation coefficient μ is represented by the sum of the individual coefficients μ_i :

$$\mu = \sum_i \mu_i \quad . \tag{B 4}$$

The transmission then becomes

$$T = e^{-\sum_i \mu_i \rho_i d} \quad , \tag{B 5}$$

where ρ_i denotes the fractional density of element i.

In Fig. B 2 we illustrate for a uranium solution how the transmission varies as a function of energy in the vicinity of the K-absorption edge. For the given example we assumed a uranium concentration of 250 g/ℓ in a matrix of 3N HNO_3. The thickness of the solution layer was assumed to be 2 cm. The figure shows 3 transmission curves : the smooth transmission curve due to the matrix component, the transmission due to uranium showing the distinct discontinuity at the K-absorption edge energy (E_K = 115.6 keV), and the total transmission of the composite solution. The latter is just obtained as a product of the two former transmissions.

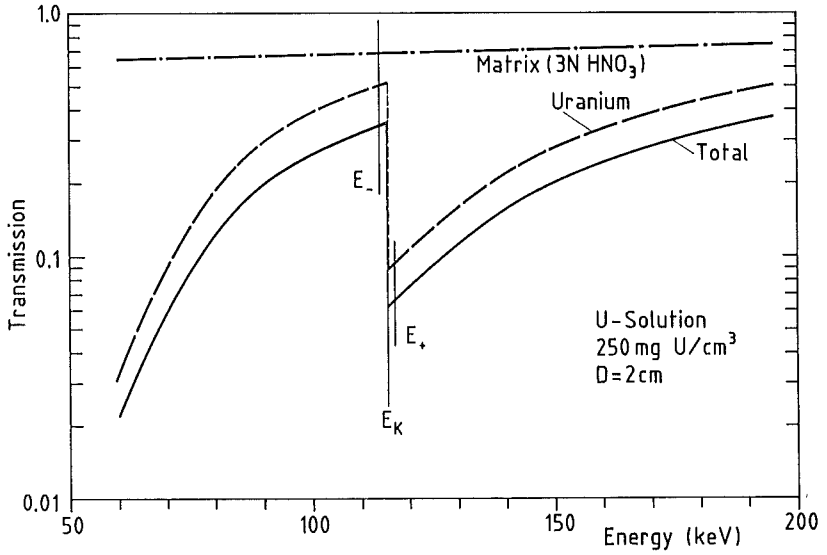

Fig. B 2 : Photon transmission as a function of energy for a uranium solution (250 g U/ℓ in 3 N HNO_3).

Within limited energy ranges the mass attenuation coefficient μ(E) can be represented by a power function :

$$\mu(E) = a\, E^{-b} \quad . \tag{B 6}$$

Inserting (B 6) into (B 3) and taking the logarithm we obtain

$$\ell n\, T = -a\, E^{-b} \cdot \rho \cdot d \tag{B 7}$$

and

$$\ell n\, \ell n\, 1/T = \ell n\, a\rho d - b\, \ell nE = a - b\, \ell nE \quad . \tag{B 8}$$

Note that in this representation the double logarithmic 1/T - values become linear versus ℓn E as shown in Fig. B 3. In this way linear least - squares fit can be

made to the measured transmission values below and above the absorption edge in order to determine the ratio of transmissions across the K-absorption edge.

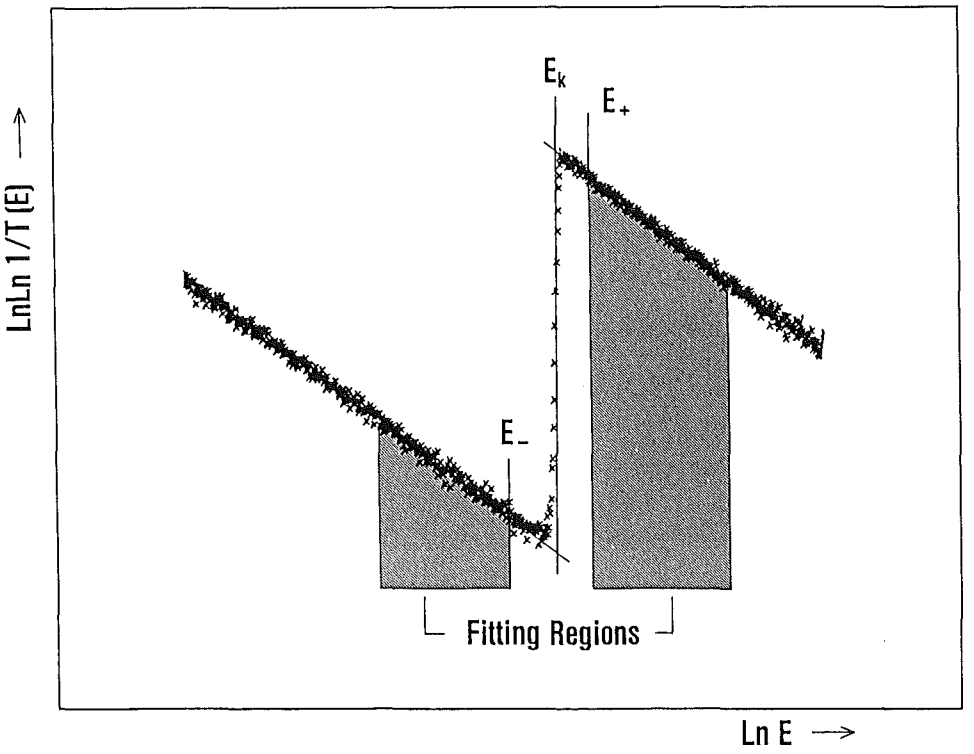

Fig. B 3 : Values ℓn ℓn 1 / T(E) plotted versus ℓn E around the K - absorption edge.

Appendix C. **Densitometry Equation**

The fractional density of an analyte, ρ_A, in a matrix of density ρ_M can be determined selectively from transmission measurements below and above the absorption edge energy of the analyte. We denote the energies on both sides of the absorption edge, where the transmission is determined, with E- and E_+ (see Fig. B 2).

For a sample of thickness d we obtain from Eq. B 5

$$T(E_-) = exp - [\,\mu_A(E_-)\,\rho_A + \mu_M(E_-)\,\rho_M\,]\,d \qquad \text{(C 1)}$$

$$T(E_+) = exp - [\,\mu_A(E_+)\,\rho_A + \mu_M(E_+)\,\rho_M\,]\,d \quad , \qquad \text{(C 2)}$$

where μ_A and μ_M represent the mass attenuation coefficient of the analyte and the matrix at the transmission energy. The ratio of the transmissions calculates from C 1 and C 2 to

$$T(E_-)/T(E_+) = exp\,[\,\Delta\mu_A\,\rho_A - \Delta\mu_M\,\rho_M\,]\,d \quad , \qquad \text{(C 3)}$$

with

$$\Delta\mu_A = \mu_A(E_+) - \mu_A(E_-)$$

$$\Delta\mu_M = \mu_M(E_-) - \mu_M E_+) \; .$$

Solving the logarithmic ratio

$$\ell n\left[\,T(E_-)\,/\,(TE_+)\right] = [\,\Delta\mu_A\,\rho_A - \Delta\mu_M\,\rho_M\,]\,d$$

for ρ_A yields

$$\rho_A = \frac{\ell n\left[\,T(E_-)/T(E_+)\right]}{\Delta\mu_A\,d} + \frac{\Delta\mu_M}{\Delta\mu_A}\,\rho_M \; . \qquad \text{(C 4)}$$

For the general case we have to include into the matrix term the sum over all elements in the sample excluding the analyte :

$$\rho_A = \frac{\ell n\left[\,T(E_-)/T(E_+)\right]}{\Delta\mu_A\,d} + \frac{1}{\Delta\mu_A}\sum_{i\neq A}\Delta\mu_i\,\rho_i \; . \qquad \text{(C 5)}$$

There are experimental possibilities to eliminate the matrix term in Eqs. C 4 and C 5, which reduces the densitometry equation to the simple form

$$\rho_A = \frac{\ell n\left[\,T(E_-)/T(E_+)\right]}{\Delta\mu_A \cdot\; d} \; . \qquad \text{(C 6)}$$

In Eq. C 6 the quantities ρ_A, $\Delta\mu_A$ and d are expressed in units [g·cm^{-3}], [cm^2·g^{-1}] and [cm], respectively. To obtain the concentration in units of g/ℓ, Eq. C 6 must be multiplied by a factor of 1000 :

$$\rho_A\,(g/\ell) = \frac{\ell n\left[\,T(E_-)/T(E_+)\right]}{\Delta\mu_A \cdot\ d} \cdot\ 1000\ . \qquad \text{(C 7)}$$

One way to eliminate the matrix term is to measure the ratio of the transmissions exactly at the absorption edge energy E_K, approaching a situation where $E- = E_+ = E_K$. In this case the difference of the mass attenuation coefficients $\Delta\mu_i = \mu_i\,(E-) - \mu_i\,(E_+)$ becomes zero for all elements i excepting the analyte, because their attenuation coefficient $\mu_i\,(E)$ shows a smooth behaviour at the absorption edge energy of the analyte. Hence, with $\Delta\mu_i = 0$, the matrix term in Eqs. C 4 and C 5 vanishes. This approach is realized in practice by measuring the transmissions below and above the edge as a function of energy, and to extrapolate them from both sides to the absorption edge energy.

If one has adopted the former procedure of determining the transmissions at energies E- and E_+ which are slightly displaced from the absorption edge energy E_K, the matrix term can be eliminated - or greatly reduced - when the measurements are normalized to a reference measurement from a blank sample. Since the transmission T_S for the sample, composed of the analyte and the matrix, is

$$T_S = T_A \cdot T_M\ ,$$

the matrix term will vanish when referencing T_S to the transmission T_M from a blank sample of identical matrix composition. If the matrix composition in the sample differs from that of the reference sample, the matrix term in Eq. C 5 takes the form

$$\frac{1}{\Delta\mu_A} \sum_{i \neq A} \Delta\mu_i\,\Delta\rho_i\ ,$$

where $\Delta\rho i = \rho_i$ (Sample) $- \rho_i$ (Reference) represents for matrix element i the difference between its density in the actual sample and in the blank reference sample used for normalization.

To illustrate the magnitude of matrix effects in K-edge densitometry we give two numerical examples, referring to the determination of the uranium concentration in a nitrate solution. Let us assume that the reference spectrum had been taken from a blank 3 N HNO_3 solution, and that the transmission below and above the K-absorption edge of uranium are measured at energies $E- = E_K -$ 2.4 keV and $E_+ = E_K$ + 1.6 keV (as it is done in the Hybrid Instrument).

Example 1 . We assume that the matrix of the uranium sample to be measured is also 3 N HNO_3, but that it contains in addition 1% of plutonium relative to uranium. According to the matrix term in Eq. C 4 the bias on the uranium assay then calculates to

$$\frac{\Delta\mu_{Pu}}{\Delta\mu_U} \cdot \rho_{Pu} = \frac{0.125}{3.31} \cdot 0.01\,\rho_U = 3.8 \cdot 10^{-4}\rho_U \ ,$$

where the numerical values for $\Delta\mu$ were interpolated from tabulated photon mass attenuation coefficients /6/. Thus, the presence of 1% plutonium will lower the measured uranium concentration by 0.04%.

Example 2. We assume that the matrix of the uranium sample is 8 N HNO_3 instead of 3 N HNO_3 as used in the blank reference sample. With the difference $\Delta\rho_M = 0.05$ between the densities of the two HNO_3 molarities the matrix term then calculates to

$$\frac{\Delta\mu_M}{\Delta\mu_U}\,\Delta\rho_M = \frac{1.77 \cdot 10^{-3}}{3.31} \cdot 0.05 = 2.7 \cdot 10^{-5} \ .$$

In relation to a uranium concentration of 200 g U/ℓ ($\rho_U = 0.2$) the increased matrix density will cause a negative bias of about 0.013% in the uranium assay. If the matrix density in the sample is smaller than in the reference sample, the measurement will positively be biased.

Appendix D. **Characteristic X - Rays**

Characteristic X-rays are emitted upon a photoelectric interaction which preferably occurs on the tightly bound inner-shell electrons (K, L, M) of an atom. The process leading to the emission of characteristic X-rays is illustrated in Fig. D 1. In the figure the incident radiation (a photon or a charged particle) has

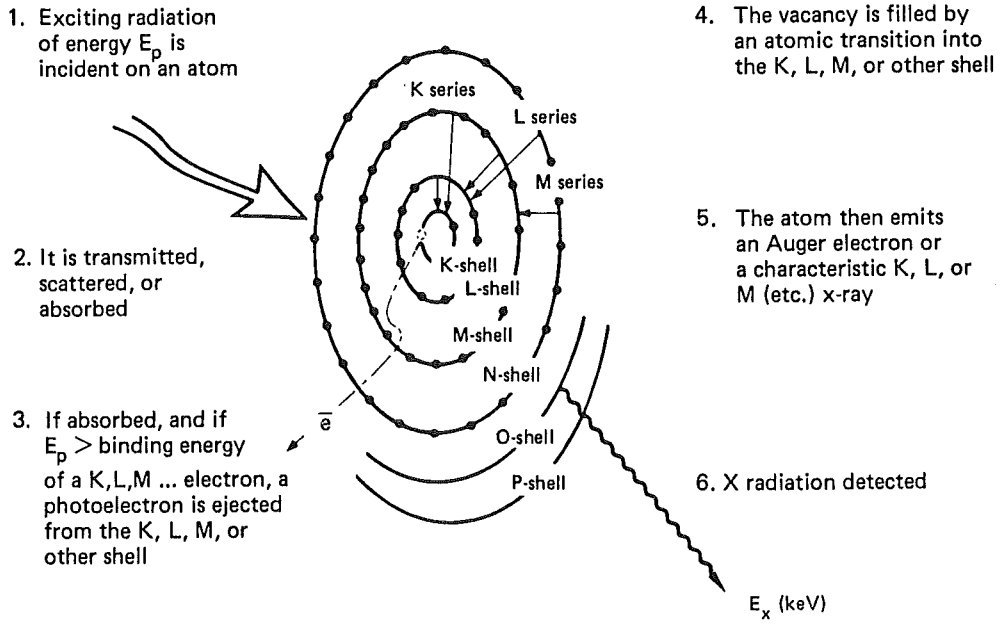

Fig. D 1 : Illustration of the physical phenomenon leading to the emission of characteristic X-rays (taken from Ref. 11).

ejected one of the K electrons. The vacancy left in the K-shell represents an unstable situation. Consequently, an electron from an outer shell will transfer to the K-shell to fill the vacancy. The difference in electron binding energies between the two shells can be given off in the form of a characteristic X-ray photon, or of an electron (called Auger electron).

The probability for X-ray emission is described by the fluorescence yield ω. The fluorescence yield lies between 0 and 1. Characteristic X-ray emission becomes more probable for high-atomic-number elements, whereas Auger electron emission is more probable for low-atomic-number elements. For K-shell ionization we find $\omega_K = 0.976$ for U and $\omega_K = 0.977$ for Pu.

The energies of the characteristic X-rays are a unique signature for each element. In the Hybrid Instrument we make use of K series X-rays from U and Pu.

Fig. D 2 shows the electron levels in a uranium atom with the possible electron transitions into a K-shell vacancy, leading to the emission of K X-rays.

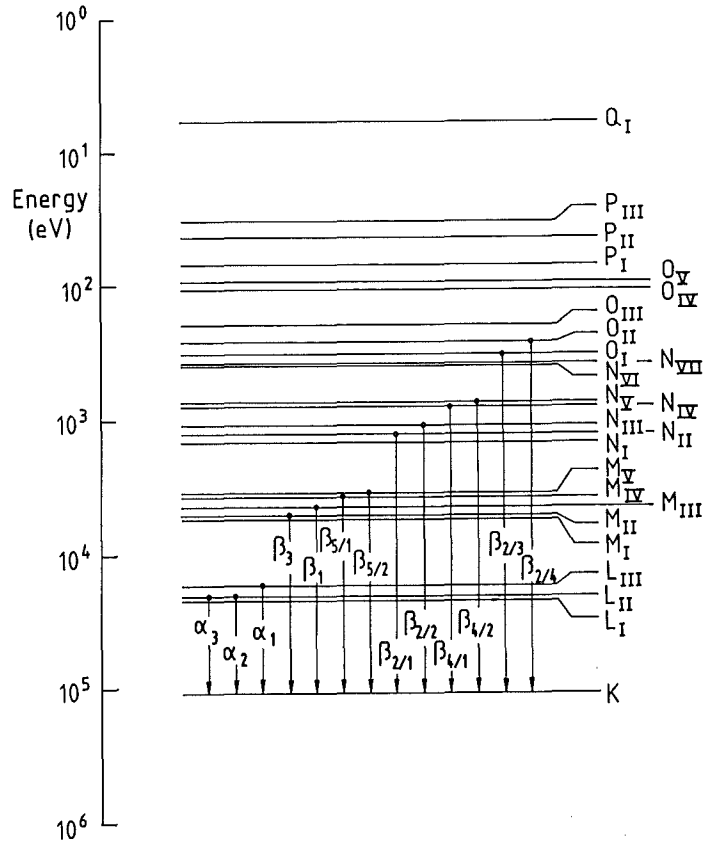

Fig. D 2 :

Atomic levels of uranium with K series X-rays.

The energy scale in the figure represents the electron binding energy in the different shells. Each of the indicated transitions has a fixed probability. The transition from the L_{III} to the K-shell, denoted by α_1, is the most abundant one.

Table D 1 lists the energies and relative intensities of the K series X-rays from U and Pu. The relative intensities are normalized to a value of 100 for the most abundant α_1 - transition.

The typical appearance of a K series X-ray spectrum - measured with a Ge-detector spectrometer - is reproduced in Fig. D 3. The spectrum resulted from the excitation of a uranium sample by means of photons from a ^{57}Co source. We observe the two well resolved $K\alpha_1$ and $K\alpha_2$ lines, and two partly resolved peak complexes containing the $K\beta_{1,3,5}$ and $K\beta_{2,4}$ X-rays.

Note from the figure the characteristic line shape of the X-rays, which differs from the line shape of a gamma ray. K X-rays from very high-atomic number elements such as U and Pu have a natural line width of about 100 eV with a Lorentzian profile. The experimentally observed line shape represents a convolution of this Lorentzian profile with the Gaussian-like profile describing the detection process in the detector. This is illustrated in Fig. D 4.

Table D 1 : K Series X-Rays of Uranium and Plutonium

Designation of X-ray	Transition	Energy (keV)		Relative Intensity	
		U	Pu	U	Pu
α_3	$L_I \rightarrow K$	93.847	98.688	0.231	0.264
α_2	$L_{II} \rightarrow K$	94.658	99.527	62.6	63.0
α_1	$L_{III} \rightarrow K$	98.436	103.734	100.	100.
β_3	$M_{II} \rightarrow K$	110.425	116.242	11.6	11.7
β_1	$M_{II} \rightarrow K$	111.302	117.229	22.6	22.8
$\beta_{5/1}$	$M_{IV} \rightarrow K$	111.878	117.824	0.403	0.424
$\beta_{5/2}$	$M_V \rightarrow K$	112.054	118.019	0.460	0.478
$\beta_{2/1}$	$N_{II} \rightarrow K$	114.333	120.414	2.89	2.95
$\beta_{2/2}$	$N_{III} \rightarrow K$	114.561	120.667	5.83	5.95
$\beta_{4/1}$	$N_{IV} \rightarrow K$	114.826	120.948	0.255	0.272
$\beta_{4/2}$	$N_V \rightarrow K$	114.866	120.996		
$\beta_{2/3}$	$O_{II} \rightarrow K$	115.341	121.497	2.07	2.20
$\beta_{2/4}$	$O_{III} \rightarrow K$	115.411	121.580		

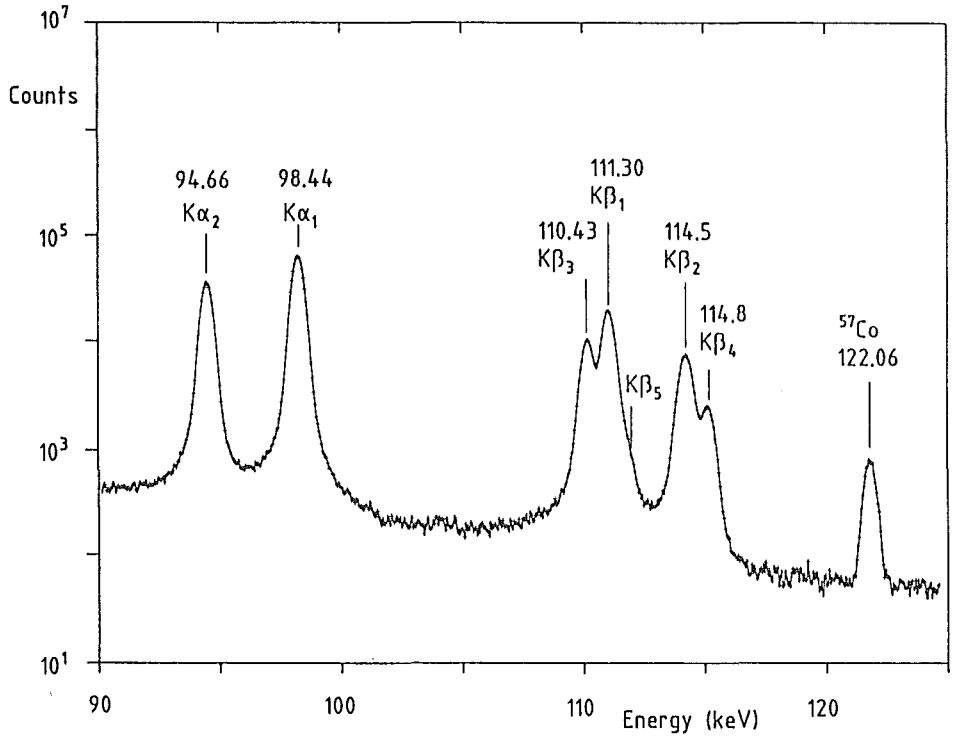

Fig. D 3 : Spectrum of K X-rays from uranium.

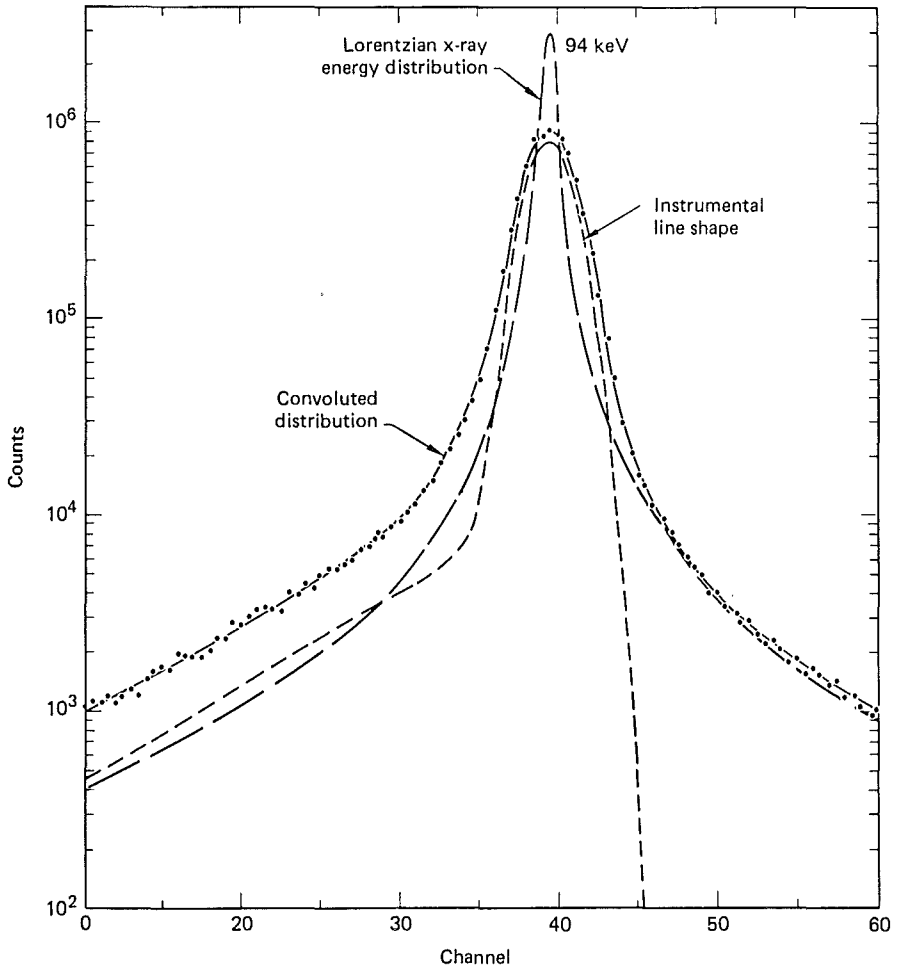

Fig. D 4 : Line shape of K X-rays, illustrated for the UKα2 X-ray (taken from Ref. 7).

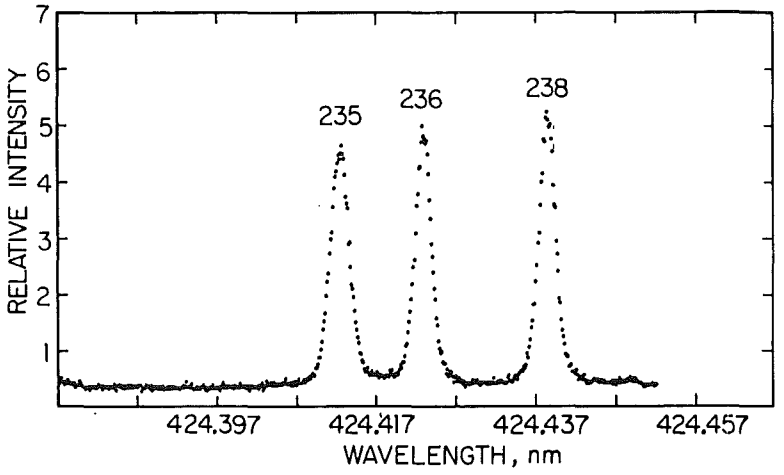

Fig. D 5 : Isotope effect for the 424 nm transition in doubly ionized uranium atoms (taken from Ref. 12).

The electron binding energy in atomic shells - and hence the transition energies between shells - can be slightly different for isotopes of a given element. This *isotope effect* is observed with highest resolving spectrometers in optical emission spectroscopy. A nice example for this is given in Fig. D 5. Note from the abscissa that the isotope shift is very small ($\Delta E/E \sim 10^{-5}$). This small effect is principally not detectable in X-ray spectrometry because of the relatively large natural line width of X-rays. We therefore note : X-ray spectrometry is an *element but not isotope-specific* measurement technique.

Appendix E. **X - Ray Continuum (Bremsstrahlung)**

The Hybrid Instrument employs an external beam of X-rays to probe the input sample. This external beam is an X-ray continuum generated as bremsstrahlung in an X-ray tube.

Fig. E 1 shows a cross - sectional view of the X-ray tube used in the Hybrid Instrument. Electrons emitted by a heated cathode are accelerated through a negative potential and focussed to strike the anode (here tungsten). In our application a negative potential of 150 kV is applied to the cathode (filament), and the electron beam current is 15 mA. Each electron, when it reaches the anode, has acquired a kinetic energy of 150 keV.

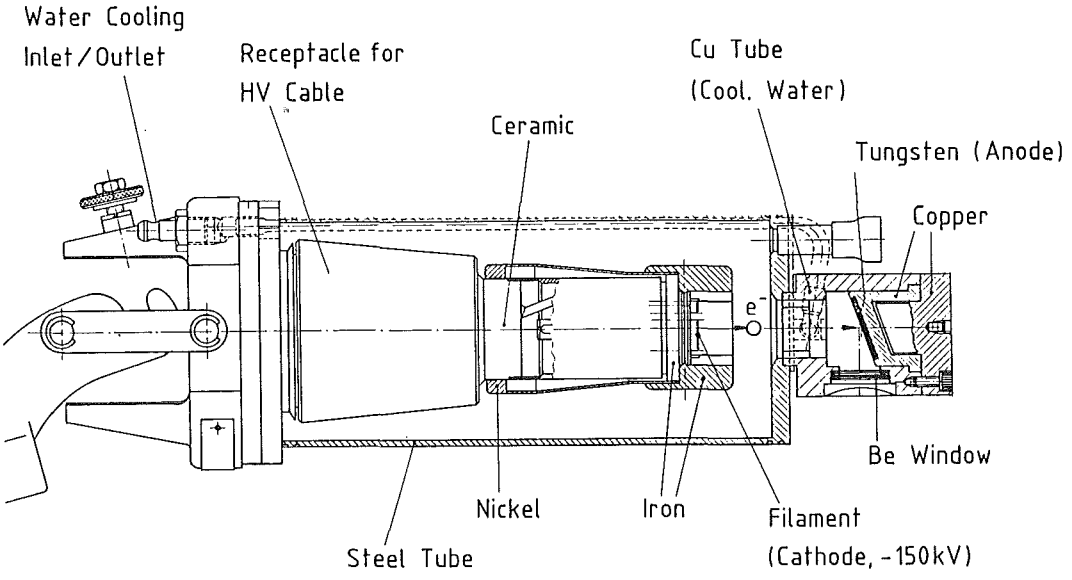

Fig. E 1 : Cross-sectional view of the X-ray tube used in the Hybrid Instrument.

Most of the power (2.25 kW) transferred to the accelerated electrons is dissipated as heat in the anode, which has to be removed by water cooling. Only a small fraction of the power results in the emission of X-rays. The X-rays are produced in a small fraction of the cases where the electron is deflected by atomic nuclei in the anode. The energy of the generated X-ray photon can vary from zero up to the full energy of the incident electron. Thus, a continuum of X-ray photon energies is generated referred to as *bremsstrahlung*.

Fig. E 2 shows the energy distribution of X-ray photons emitted from an X-ray tube with a thick tungsten target. The spectrum represents an actually measured distribution from a tube operated at 140 kV /13/. We note that characteristic X-rays from the tungsten anode material are superimposed to the bremsstrahlung continuum.

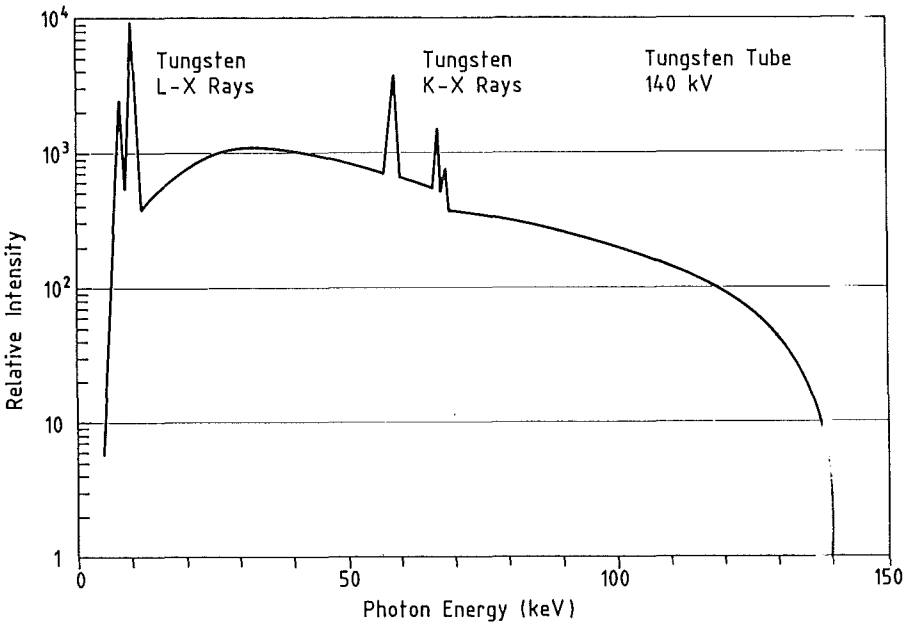

Fig. E 2 : Distribution of X-ray photon energies generated from an X-ray tube with thick tungsten target.

The upper portion of the bremsstrahlung continuum ($E > 70$ keV) can fairly well be described analytically. The number of X-rays emitted per unit time dt and unit solid angle $d\Omega$ in the photon energy interval E to $E + dE$ is calculated from the thick-target bremsstrahlung formula

$$\frac{d^3N(E)}{dt\,dE\,d\Omega} = Q(E, E_0, Z) \cdot R(E, E_0) \cdot f(E, E_0, Z) \cdot I. \qquad \text{(E1)}$$

In Eq. E1 $Q(E, E_0, Z)$ represents the source term describing the distribution of X-rays generated from the deacceleration of electrons with initial energy E_0 in the target (anode) with atomic number Z ($Z = 74$ for tungsten). The terms $R(E, E_0)$ and $f(E, E_0, Z)$ are correction factors accounting for the loss of electrons due to backscattering from the target surface and for the attenuation of the X-rays in the target, respectively. I denotes the tube current.

Weise et al. /5/ found fairly good agreement between calculated and measured bremsstrahlung spectra when choosing for the source term $Q(E, E_0, Z)$ the semi-empirical formula

$$Q(E, E_0, Z) = C \cdot Z \left[\frac{E_0}{E} - 1 \right] / \left(\frac{E}{E_K} \right)^{1/3}, \qquad \text{(E2)}$$

where E_K denotes the K-absorption edge energy of the target material (E_K = 69.53 keV for tungsten). The constant C was determined from fits to experimental data to

$$C = 1.41 \cdot \ 10^9 mA^{-1} s^{-1} keV^{-1} sr^{-1}, \tag{E3}$$

whereby the correction terms $R\ (E, E_0)$ and $f\ (E, E_0, Z)$ had been approximated by the relations

$$R\ (E, E_0) \approx 1 - 0.43 \left(1 - \frac{E}{E_0}\right)^{0.356} \tag{E4}$$

$$f(E, E_0, Z) \approx exp - \left[0.2\, r(E_0, Z) \cdot \ \mu(E) \cdot \ tan^{-1} \alpha\right]. \tag{E5}$$

In Eq. E 5 the quantity $r\ (E_0, Z)$ represents the maximum range of electrons with energy E_0 in the tungsten target, and $\mu(E)$ its total linear photon attenuation coefficient. The target angle α is defined as angle between the incident electron beam and the normal to the target (Fig. E 3). For the present tube we have α = 23°. The same angle is also subtended between target surface and X-ray beam direction in the Hybrid Instrument, where the extracted X-ray beam is perpendicular to the electron beam.

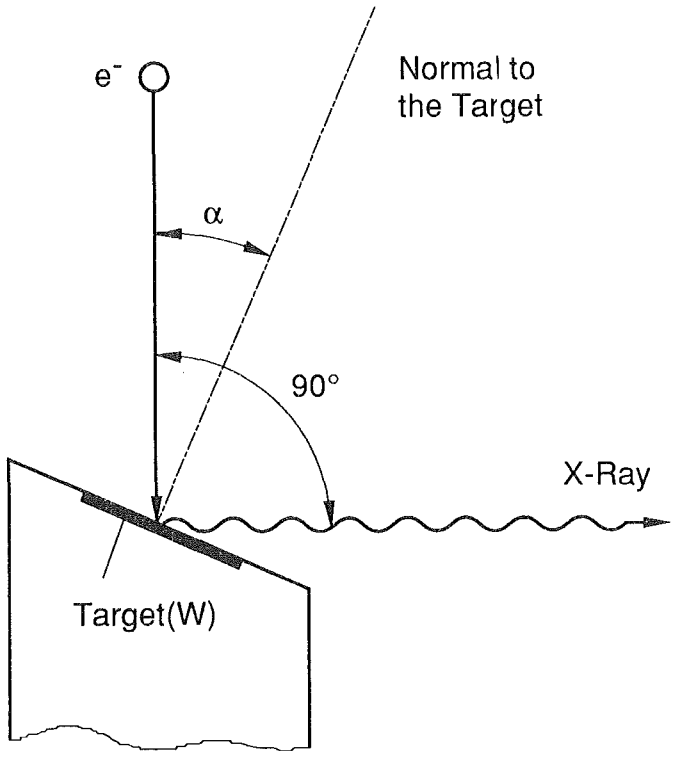

Fig. E 3 : Beam and target geometry.

The analytical expression for the thick-target bremsstrahlung distribution, based on Eqs. E 1 to E 5, was used to calculate the ratio of the X-ray production from uranium and plutonium, $R_{U/Pu}$, as a function of the total heavy element concentration in the sample. To this end the bremsstrahlung distribution had to be folded with the photoelectric cross-sections of the two elements in the energy interval between the K-absorption edge energy E_K and the endpoint energy E_0, taking into account the energy-dependent beam attenuation in the sample and in the beam filters. These calculations were carried out for different uranium concentrations at a fixed U/Pu ratio of 100. The exponential term appearing in the expression for the XRF calibration factor $R_{U/Pu}$ (Eq. 17 in Section 4.3.2 and Eq. H 2 in Appendix H) has been established from a least-squares fit to a set of data points calculated in this way.

Further, the bremsstrahlung formula was also used to calculate the dependence of the calibration factor $R_{U/Pu}$ on the tube voltage setting as shown in Fig. 24 in Section 4.4.4.

Appendix F. **Energy Loss in Inelastic Scattering**

The majority of both the elastic and inelastic photon scattering arises from the loosely bound outer-shell electrons. Scattering does not provide any element-specific information, and it represents a cumbersome and disturbing effect in X-ray spectrometry. Inelastically scattered photons have lost some of their initial energy. The energy E' of an inelastically scattered photon with initial energy E_0 is

$$E' = \frac{E_o}{1 + \frac{E_o}{m_o c^2}(1 - \cos\theta)} , \qquad \text{(F 1)}$$

where θ is the scattering angle, and m_0c^2 = 511.006 keV the electron rest mass. Eq. F 1 was established by Compton, so inelastic photon scattering often is also referred to as Compton scattering.

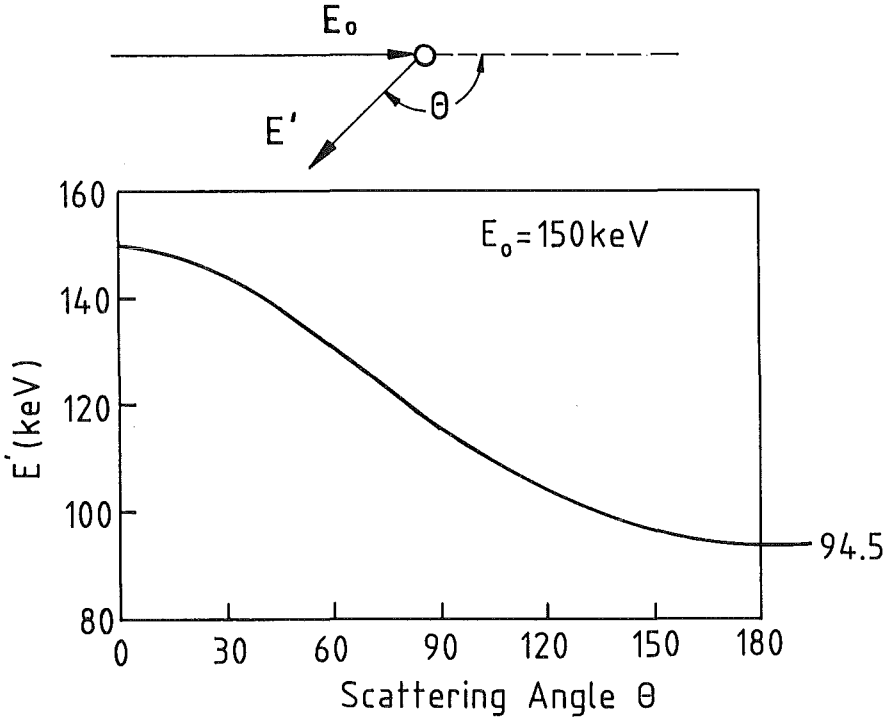

Fig. F 1 : Energy of inelastically scattered photons with initial energy E_0 = 150 keV as function of scattering angle.

Fig. F 1 shows how the scattered photon energy E' of an incident photon with energy E_0 = 150 keV decreases with increasing scattering angle. For scattering angles $\theta \geq 150°$ the energy loss E_0 - E' is about 50 keV. This means that the X-ray continuum shown in Fig. E 2, when inelastically scattered on a sample and observed at backward angles, will be shifted towards lower energies by about

50 keV. This is the physical reason why in the Hybrid Instrument the XRF detector is located at the largest possible backward angle ($\theta = 150°$) relative to the direction of the primary X-ray beam. For this beam geometry primary X-rays with energies up to 150 keV, when inelastically scattered from the sample, arrive at the XRF detector with a maximum energy of about 100 keV.

This fact leads to the important practical consequence that the inelastically scattered primary X-rays are removed from the energy region where the characteristic K X-rays from uranium and plutonium occur. The signal-to-background ratio for these X-rays becomes in this way drastically improved as illustrated in Fig. F 2. In the given example, where the tube was operated at 145 kV and the XRF detector was oriented at 157° relative to the direction of the primary beam incident on the sample, the onset of the scattering bump occurs at about 94 keV.

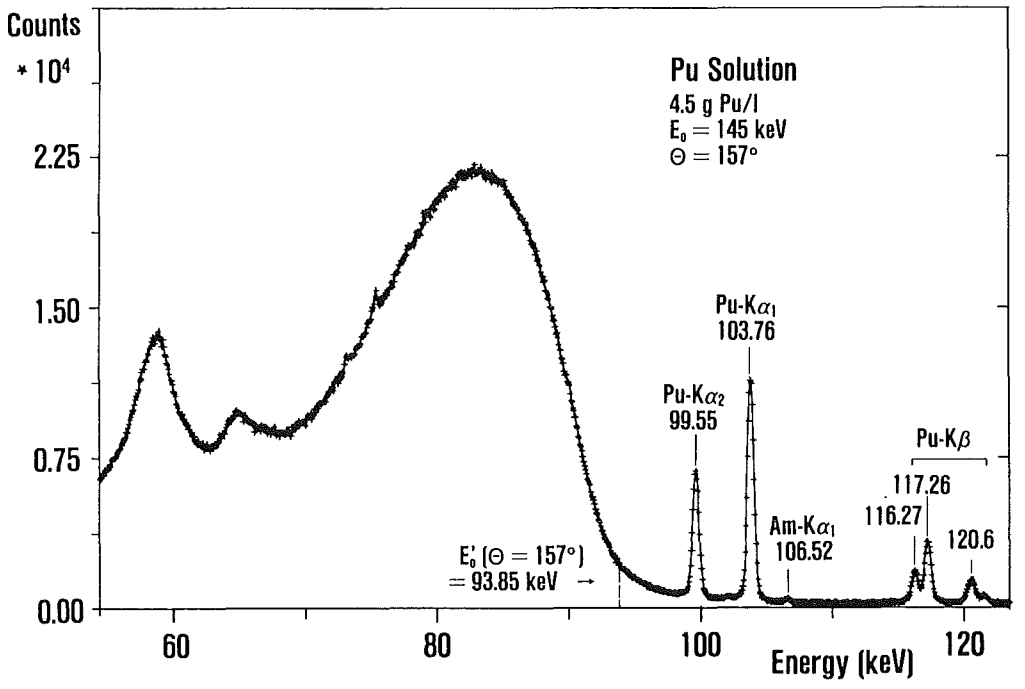

Fig. F 2 : Reduction of scattering background for plutonium K X-rays.

For the operating conditions of the Hybrid Instrument at La Hague (150 kV, $\theta = 150°$) the energy of inelastically scattered X-rays extends up to about 98 keV. This situation still allows the spectroscopy of the $K\alpha_1$ X-ray from the minor element plutonium at favorable peak-to-background ratios as shown for the measurement examples in Fig. F 3.

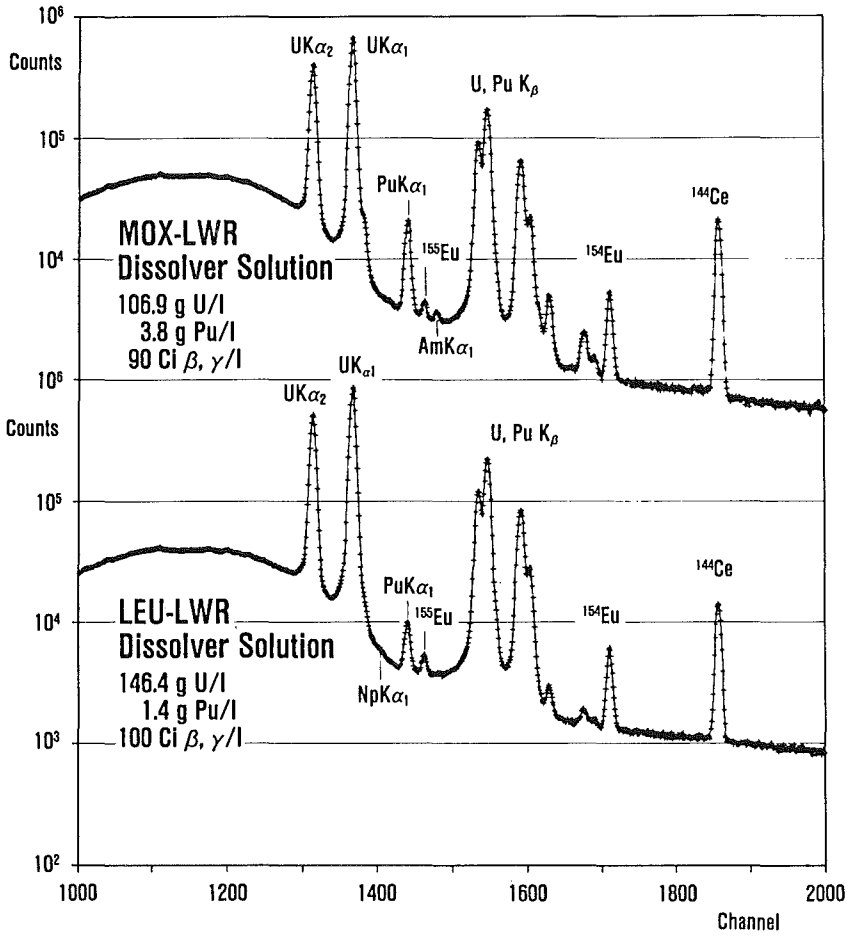

Fig. F 3 : K - XRF spectra measured with the Hybrid Instrument from LEU - LWR and MOX - LWR dissolver solutions.

Appendix G. **Composition of Dissolver Solutions**

Dissolver solutions from spent nuclear fuels are special and difficult materials for two reasons. First, they are chemically very complex samples, containing about 40 to 50 different elements. Second, they are highly radioactive, exhibiting a high radiation dose. In fact, undiluted dissolver solutions exhibit the highest radiation dose among the samples presently handled for safeguards verification measurements. This necessitates sample handling in well-shielded facilities.

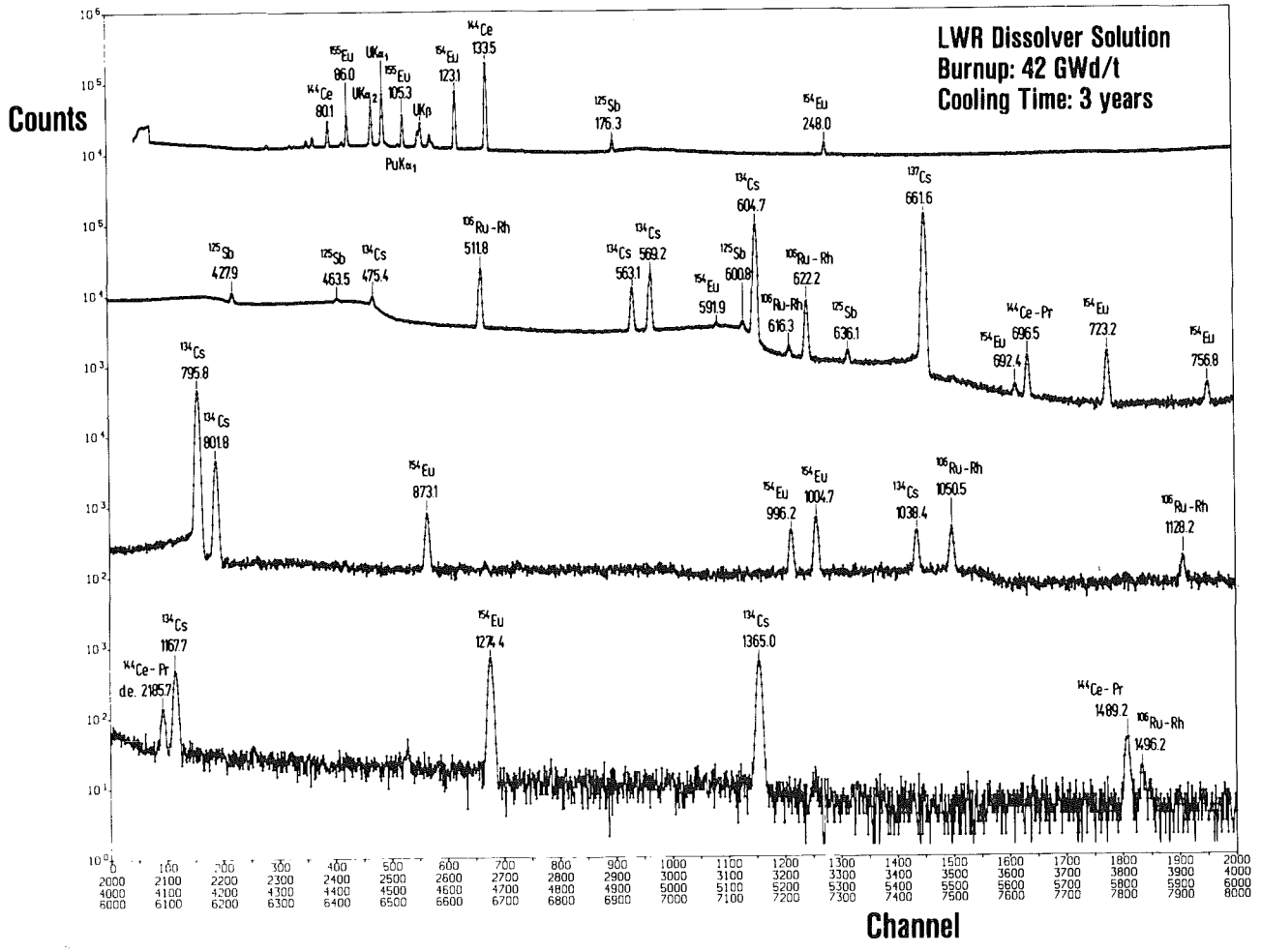

Fig. G 1 : Gamma spectrum from an input solution.

Table G 1 lists the typical concentrations of fission products and actinides in dissolver solutions. The values are based on burnup calculations using the code KORIGEN /14/. They were normalized to a value of 250 g/ℓ for the major element uranium. This is a value typically found in dissolver solutions. Some of the fission products such as Zr, Mo, Ru, Tc and Pd poorly dissolve in a nitric acid medium.

Table G 1 Concentration of Fission Products and Actinides in Dissolver Solutions.
Basis: 250 g U/ℓ, Burnup 40 GWd/t, Cooling Time 5 years.

Element	Concentration (g/ℓ)	Element	Concentration (g/ℓ)
Ge	0.0001	Xe	1.71
As	<0.0001	Cs	0.79
Se	0.0175	Ba	0.52
Br	0.0069	La	0.39
Kr	0.11	Ce	0.77
Rb	0.11	Pr	0.36
Sr	0.26	Nd	1.30
Y	0.15	Pm	0.013
Zr	1.15	Sm	0.26
Nb	< 0.0001	Eu	0.044
Mo	1.08	Gd	0.046
Tc	0.24	Tb	0.0007
Ru	0.71	Dy	0.0004
Rh	0.14	Ho	< 0.0001
Pd	0.44	Er	< 0.0001
Ag	0.020		
Ca	0.025		
In	0.0004	U	250.0
Sn	0.015	Np	0.15
Sb	0.0035	Pu	2.72
Te	0.15	Am	0.12
I	0.07	Cm	0.011

Table G 2 Activity of Major Gamma Emitting Fission Products in Dissolver Solutions.
Basis : 250 g U/ℓ, Burnup 40 GWd/t

Isotope	Half Life	Activity (Bq / ℓ)		
		Cooling Time		
		2 years	5 years	7 years
Ru - 106	368d	1.54 E + 12	1.96 E + 11	4.95 E + 10
Sb - 125	2.77a	6.58 E + 10	3.10 E + 10	1.88 E + 10
Cs - 134	2.06a	1.10 E + 12	4.03 E + 11	2.06 E + 11
Cs - 137	30.17a	1.20 E + 12	1.12 E + 12	1.07 E + 12
Ce - 144	285d	2.17 E + 12	1.50 E + 11	2.53 E + 10
Eu - 154	8.8a	1.35 E + 11	1.05 E + 11	8.99 E + 10
Eu - 155	4.96a	7.22 E + 10	4.75 E + 10	3.58 E + 10
Totals		6.28 E + 12 (170 Ci)	2.05 E + 12 (55 Ci)	1.50 E + 12 (40 Ci)

These elements are concentrated to some extent in the high active waste and will not fully appear in the clarified dissolver solution transferred to the input accountancy tank. The same is, of course, also true for the gaseous fission products such as Kr and Xe.

The dissolver solution is highly radioactive. Fig. G 1 presents a typical gamma spectrum from an input solution. It is dominated by gamma rays from a few longer-lived fission products, whose activity completely masks the natural radioactivity of the actinide elements. The presence of uranium and plutonium only manifests through their characteristic X-rays, which are excited by the intense radiations from the fission products. The passive radiations, however, do not allow a quantitative determination of uranium and plutonium.

Table G 2 lists the major gamma emitting fission products together with their activities. Again the data are based on calculations with KORIGEN /14/ for the nuclide inventory in spent LWR fuel with a burnup of 40 GWd/t. The activities were put in proportion to a uranium quantity of 250 g/ℓ. The actual total activity of the input solution in the accountancy tank will be somewhat lower than listed in the table because a few nuclides like Ru-106 and Sb-125 preferably concentrate in the high active waste stream. But it typically remains in the range of 10^{12} Bq/ℓ for the respective burnup and cooling times.

The chemically complex and highly radioactive input solution can be subject to changes with time, which may alter the uranium and plutonium concentration in either direction : evaporation, formation of chemical complexes tending to precipitate, post dissolution of undissolved residual fuel etc. It is therefore not unusual if the same sample, when measured from time to time, yields different results.

For the measurement situation at La Hague, where the received input solutions appear to be well clarified after a preceding centrifugation, the most likely effect causing a change of the samples is evaporation. This may particularly occur - and it has been already observed - after the transfer of the input solution into the sample vials for measurement. It is therefore recommended to analyze the input solution as soon as possible and not to store them for longer periods in the vials before measurement.

Appendix H. **Calibration of the XRF Measurement for the U/Pu Ratio**

Prior to its shipment to La Hague the Hybrid Instrument has been calibrated at KfK with synthetic U/Pu - solutions prepared by TUI, Karlsruhe. During the calibration runs it was found, however, that the reference solutions - because of evaporation - must have slightly changed their concentration. For this reason a reliable calibration for the KED branch, which measures absolute uranium concentrations, was not possible at that time. Therefore we have taken over, as an initial calibration for KED, the calibration constant from another Hybrid Instrument. According to previous experiences it was expected that this calibration constant from an instrument of similar design should also apply to the present instrument within an uncertainty of about 0.1 - 0.2 % (this assumption has been verified during a final calibration carried out in July 1990).

Below we list the calibration results for the XRF branch, which for the analysis of input solutions just has to be calibrated for the U/Pu ratio measurement. For this calibration we made the reasonable assumption that the small changes of the absolute concentrations in the reference samples due to evaporation did not alter the U/Pu ratio.

Table H 1 : Reference Solutions

Solution No.	U (g/ℓ)	Pu (g/ℓ)	U/Pu Ratio
1	252.061	2.5411	99.193
2	200.692	2.0198	99.360
3	150.978	1.4969	100.861
4	100.462	0.9906	101.416

H 1. Reference Solutions

The synthetic U/Pu - solutions were prepared on a gravimetric basis from Pu metal standard material NBS 949e and U metal standard material NBS 960. The reference materials were dissolved in 4.5 N HNO_3 and mixed to yield solutions with a U/Pu ratio of about 100. Four different solutions, 4 mℓ each, as listed in Table H 1 were available for the calibration. The uncertainty of the given U/Pu ratio values is 0.05% at maximum. The volume concentrations, determined from an additional density measurement, were not used for the present XRF calibration.

H 2. XRF Calibration Factor

The U/Pu mass ratio determined from the XRF measurement is given by the following relation:

$$\frac{U}{Pu} = \frac{A\,(U)}{A\,(Pu)} \cdot \frac{P\,(UK\alpha_1)}{P\,(PuK\alpha_1)} \cdot \frac{ORE\,(PuK\alpha_1)}{ORE\,(UK\alpha_1)} \cdot \frac{1}{R_{U/Pu}} \qquad \text{(H 1)}$$

with

A = atomic weight for uranium and plutonium, respectively,
P = net peak area of the $K\alpha_1$ X-rays
ORE = overall relative detection efficiency for the $K\alpha_1$ X-rays,
$R_{U/Pu}$ = calibration factor describing the ratio of excitation probabilities for emission of $UK\alpha_1$ and $PuK\alpha_1$ X-rays in the primary X-ray beam.

The quantity $R_{U/Pu}$ is the calibration factor to be determined. It physically depends on the spectral distribution of the incident photon beam used for fluorescence. Since the incident spectral distribution is modified by the energy-dependent attenuation of the sample, $R_{U/Pu}$ actually is not a single constant, but a function of the sample composition. For input solutions the photon attenuation in the energy region of interest is governed by the uranium concentration. Hence, $R_{U/Pu}$ is reasonably expressed as a function of ρ_U. For the given set-up the dependence has been calculated, as mentioned in Appendix E, to

$$R_{U/Pu} = R^{\circ}_{U/Pu} \cdot \exp - (1.10224 \cdot 10^{-4} \cdot \rho_U\,[g/\ell]\,), \qquad \text{(H 2)}$$

where $R^{\circ}_{U/Pu}$ denotes the calibration factor for a blank (very dilute) sample. According to Eq. H 2 the value for $R_{U/Pu}$ decreases by about 3% when the uranium concentration increases from 0 to 300 g/ℓ.

Combining Eqs. H 1 and H 2, and solving for $R^{\circ}_{U/Pu}$, yields

$$R^{\circ}_{U/Pu} = \frac{P(UK\alpha_1)/P(PuK\alpha_1)}{U/Pu} \cdot \frac{ORE(PuK\alpha_1)}{ORE(UK\alpha_1)} \cdot \frac{A(U)}{A(Pu)} \cdot exp(1.10224 \cdot 10^{-4} \cdot \rho_U\,[g/\ell]\,).$$

(H3)

$R^{\circ}_{U/Pu}$ was evaluated using the experimental data P and ORE, and the known reference data for the U/Pu ratio and the atomic masses A. The uranium concentration was taken as determined by KED at the time of the calibration measurements. This value was slightly higher than the reported reference value because of the above mentioned sample evaporation. The difference can be seen from a comparison of Tables H 1 and H 2.

H 3. Results

Table H 2 compiles the measured and evaluated data from the calibration runs. On each sample 5 repeat measurements were carried out. The counting time chosen for the individual run was equivalent to a live time of 1000 s, which corresponded to a real time of about 1400 s.

The mean $R^{\circ}_{U/Pu}$ - values obtained from the different samples represent a homogeneous data set with a 'Between Sample Standard Deviation' of 0.04%. The grand mean of $R^{\circ}_{U/Pu}$ was determined to 1.4987 with a standard error of 0.14%. This figure physically means that for the given experimental conditions the excitation of uranium X-rays is 1.5 times more probable than the excitation of plutonium X-rays.

Table H2 Calibration Data for the XRF Calibration Factor

Sample No	U (g/ℓ)	$\frac{U}{Pu}$	$\frac{P(UK\alpha_1)}{P(PuK\alpha_1)}$	$\frac{\varepsilon(PuK\alpha_1)}{\varepsilon(UK\alpha_1)}$	$\frac{A(U)}{A(Pu)}$	Expon. Factor	$R°_{U/Pu}$
1	255.83	99.193	141.23	1.0159	0.99560	1.0286	1.4812
			142.95	1.0154			1.4986
			143.74	1.0152			1.5065
			143.51	1.0158			1.5050
			143.43	1.0152			1.5033
						mean =	1.4989
						σ =	0.69 %
2	202.28	99.360	144.13	1.0132	0.99560	1.0225	1.4962
			143.77	1.0130			1.4922
			145.68	1.0135			1.5127
			143.85	1.0135			1.4937
			144.45	1.0137			1.5002
						mean =	1.4990
						σ =	0.55 %
3	154.90	100.861	148.04	1.0112	0.99560	1.0172	1.5031
			147.83	1.0112			1.5010
			147.65	1.0155			1.5055
			146.86	1.0105			1.4901
			146.71	1.0115			1.4900
						mean =	1.4979
						σ =	0.49 %
4	103.90	101.416	151.25	1.0118	0.99560	1.0115	1.5196
			149.37	1.0118			1.5007
			147.88	1.0114			1.4852
			148.20	1.0114			1.4884
			149.38	1.0122			1.5014
						mean =	1.4991
						σ =	0.90 %
					Grand Mean		1.4987
					Std. Deviation (%)		0.62
					Std. Error of Mean (%)		0.14
					Betw. Sample Std. Dev. (%)		0.04